UNIVERSITY OF CALIFORNIA
SANTA CRUZ

THE MECHANISM OF CYTOPLASMIC STREAMING IN *DROSOPHILA MELANOGASTER* OOCYTES

A dissertation submitted in partial satisfaction of
the requirements for the degree of

DOCTOR OF PHILOSOPHY

in

MOLECULAR, CELL, AND DEVELOPMENTAL BIOLOGY

by

Corey E. Monteith

June 2015

The dissertation of Corey Monteith is approved:

_____
Professor William Saxton, chair

_____
Professor Doug Kellogg

_____
Professor William Sullivan

_____
Professor Joshua Deutsch

_____
Tyrus Miller
Vice Provost and Dean of Graduate Studies

Table of Contents

Table of Figures

Abstract

The Mechanism of Cytoplasmic Streaming in *Drosophila melanogaster* oocytes

Corey E. Monteith

Background: The transport of cytoplasmic components can be profoundly affected by hydrodynamics. A striking example is ooplasmic streaming in *Drosophila*. Forces from kinesin-1 are initially directed by a disordered meshwork of oocyte microtubules, generating slow disordered cytoplasmic flows. When microtubules shift into parallel alignment, kinesin generates fast ordered flows that mix nurse cell and oocyte cytoplasms.

Results: To understand the hydrodynamic mechanism of streaming, we used fluorescence microscopy to analyze microtubule organization and cytoplasmic flows, while using mathematical modeling to identify physical conditions that contribute to kinesin-driven self-organization. In the fast ordered state, microtubules align and undergo correlated bending in a subcortical layer. Cytoplasmic flows follow the curving microtubule paths with velocities that are slow near the cortex, faster within the microtubule layer, and fastest beneath it. FRAP and photoconversion indicate that minus-ends of the aligned microtubules are stationary relative to the cortex. Using known values for microtubule stiffness and kinesin velocity, we developed and tested a coupled hydrodynamic model that revealed key variables that can shift the system between disordered and ordered states, including: 1) the distance from the cortex at which microtubules can lie parallel to its plane, and 2) the intensity of kinesin force

on its cortical microtubule tracks, which can be controlled by cytoplasmic viscosity.

Conclusions: Cytoplasmic streaming in *Drosophila* oocytes is a result of viscous drag on moving kinesin motors that mediates equal and opposite forces on cytoplasmic fluid and on microtubules whose minus ends are embedded in the cortex. Fluid flows toward plus-ends and microtubules are forced toward stationary minus-ends. Under certain conditions, this causes microtubules to align in bending arrays, creating constantly varying directions of flow that facilitate cytoplasmic mixing

Dedication and Acknowledgements

I would first like to thank Professor Bill Saxton for being an excellent mentor and a rigorous scientist, for allowing me to do my graduate research in his lab, for yakking about science whenever possible, and for being understanding when things got tough and also giving me a kick in the butt when I needed it. I would also like to thank Professor Josh Deutsch for being a fantastic collaborator, always being incredibly patient and helpful, and giving necessary insight into the physics of our system, and to thank the other two members of my committee, Professor Bill Sullivan and Professor Doug Kellogg, for their guidance and assistance with my work. I would like to thank the rest of the Saxton lab for their contributions to my research and for being a great group of people with whom it was easy and fun to be in lab. I would particularly like to thank Donna Fullerton for being the best bay-mate as well as for conversations about streaming, Anthony Bielecki for being my only undergrad, and Steven Paniagua for assistance with Klar RNAi. Figure 3.5 is all him.

To my wife, April Arcus, without whose encouragement, editing, design assistance, incisive mind, and love I never would have made it.

To Ken Ellis, Carly Govind, Sarah Tappon, Claire Woods, Dustin Winslow, Miriam Janove, Jeremy Kreher, Caroline Matteson, Carl Blij, Stephanie Blij, and Zach Monteith for being the very best group of friends (and brother!) I could imagine.

And finally, to my mom, Nancy Haber, who has always been my biggest supporter and advisor, and my dad, Leonard Monteith, who encouraged me from the start to think deeply, observe everything carefully, and always ask more questions.

Chapter 1

Introduction

Cytoplasmic Streaming

Cytoplasmic streaming is a process that occurs in many different organisms in all kingdoms of *Eukaryota,* involving the movement of the viscous internal fluid of the cell by cytoskeleton and motor proteins. It has fascinated scientists for hundreds of years, ever since it was first discovered in plant cells in the late 1700s. However, it was not until recently that the molecular players behind streaming began to be understood. This work seeks to further elucidate the physical processes of the mechanism of streaming: how molecular motors and cytoskeleton work together to produce force on the viscous cytoplasm and allow the mixing of nurse cell cytoplasm and ooplasm in the *Drosophila* oocyte.

Historical Context of Cytoplasmic Streaming

The discovery of intracellular cytoplasmic convection, called cytoplasmic streaming, protoplasmic streaming, or, in plants, cyclosis, is credited to Bonaventure Corti in 1774 (Pfeffer 1906); (Kamiya 1959); (Loewy 1949), in his observation that the stonewort plant *Chara* showed a circular movement of what he believed to be the sap (Corti 1774). A few years later these observations were repeated by Fontana (1781). These movements were forgotten until 1811, when they were rediscovered L. C. Treviranus and later in 1819 by Giovanni Battista Amici (Sharp 1921), an Italian

astronomer, microscopist, and botanist, who is best known for making improvements in the mirrors used in light microscopy. Amici observed "transparent globules" moving in the fluid, and that the fluid in the stem moved in two separate streams going in different directions. When one stream was cut into, the other stream kept flowing. Amici attributed this movement to galvanic agency (Brewster and Jameson 1829). Robert Brown discovered a more complex form of protoplasmic streaming in the stamen hairs of *Tradescantia* in 1831 (Sharp 1921), and Meyen too studied protoplasmic streaming in the same year and attributed it to the power of the fluid itself, as he could not detect any organs that moved the fluid. He was reminded of the movement of the planets around the sun and referred to streaming as "a gravitation of plants" (Conklin 1940).

As streaming continued to be studied, it was discovered that forces outside the plant cells could affect the movement of the fluid. Nägeli discovered that temperature had a direct relationship on the velocity of streaming in 1860 (Nägeli 1860), and Kühne found oxygen was essential for streaming, although further research showed that a plant could be deprived of oxygen for a prolonged period of time and streaming was not affected (Ewart 1896); (Kühne 1897); (Ritter 1899). Other external stimuli tested included light, electricity, and magnetic force. Streaming would stop entirely, or move more slowly, or only occur in certain localities within the organism or the cell (Allen and Allen 1978); (Ewart and Gotch 1903); (Kamiya 1981); (Nachmias 1969). Ewart noted that it was rare that streaming continued during the entire

existence of the adult cell, and in those cases, if there is no streaming, the cell is fatally injured (Ewart and Gotch 1903).

Despite being studied extensively over the span of the next two hundred years, the motive force behind cytoplasmic streaming remained a mystery. Many different theories were offered but it was not until 1956 that a seminal paper came out that first began to shed light on the molecular mechanism of cytoplasmic streaming, by proposing that it might be possible that the motive force was mechanical and located on the interface between the streaming cytoplasm and stationary structures beside it (Kamiya and Kuroda 1956). Soon after, bundles of microfilaments were discovered at this interface (Kamitsubo 1966); (Nagai and Rebhun 1966). When these actin bundles were disrupted, streaming was disturbed; once the bundles were allowed to regenerate, streaming resumed normal velocity (Kamitsubo 1972). This movement was then attributed to myosin in later studies (Kamiya and Kuroda 1975); (Shimmen and Tazawa 1982).

While cytoplasmic streaming was initially discovered and studied in plants, fungi, and various protists, more recent research has shown that it is present in animal cells as well, although in animals it is often restricted to certain cell types at specific time points. In most animals studied, cytoplasmic streaming takes place in early development. It is seen in the one-cell *C. elegans* embryo, where flows moving in opposite directions are coupled in order to pull the male and female pronuclei together (Niwayama and Kimura 2012), as well as during oogenesis in the gonad core to load mRNA and proteins made by oocytes in earlier stages of development into

transcriptionally and translationally quiescent oocytes in later stages of development (Wolke, Jezuit et al. 2007). Streaming also occurs in one-cell mouse embryos, where it functions to hold the meiotic spindle against the cortex of the embryo, to allow for asymmetric division of the oocyte and the polar body once fertilization has taken place (Yi, Unruh et al. 2011); (Yi, Rubinstein et al. 2013). In *Drosophila*, streaming takes place during oogenesis, mixing an influx of cytoplasm from nurse cells, which make mRNA and proteins that the egg will need to function.

Microtubules and Motor Proteins

Cytoplasmic streaming in most organisms is mediated by actin and myosin; however, in *Drosophila melanogaster*, it is driven by microtubules (Gutzeit and Koppa 1982) and Kinesin-1 (Palacios and St. Johnston 2002). Microtubules are long, polarized cytoskeletal filaments that are composed of alpha and beta tubulin dimers laid head to tail (Amos and Klug 1974). Because of the differences in the speed of polymerization between the alpha and beta subunits, one end of the microtubule grows faster when polymerizing—this is referred to as the plus end, while the more slowly-growing end is referred to as the minus end (Desai and Mitchison 1997); (Allen and Borisy 1974). There are two families of motor proteins that walk hand-over-hand unidirectionally along microtubules by hydrolyzing ATP: kinesins and dyneins. Kinesins are plus-end directed motors while dyneins are minus-end directed motors. Kinesin-1, the canonical kinesin, was the first to be discovered (Vale, Reese et al. 1985). It consists of a dimer of two kinesin heavy chain (Khc) subunits. Kinesin heavy chain

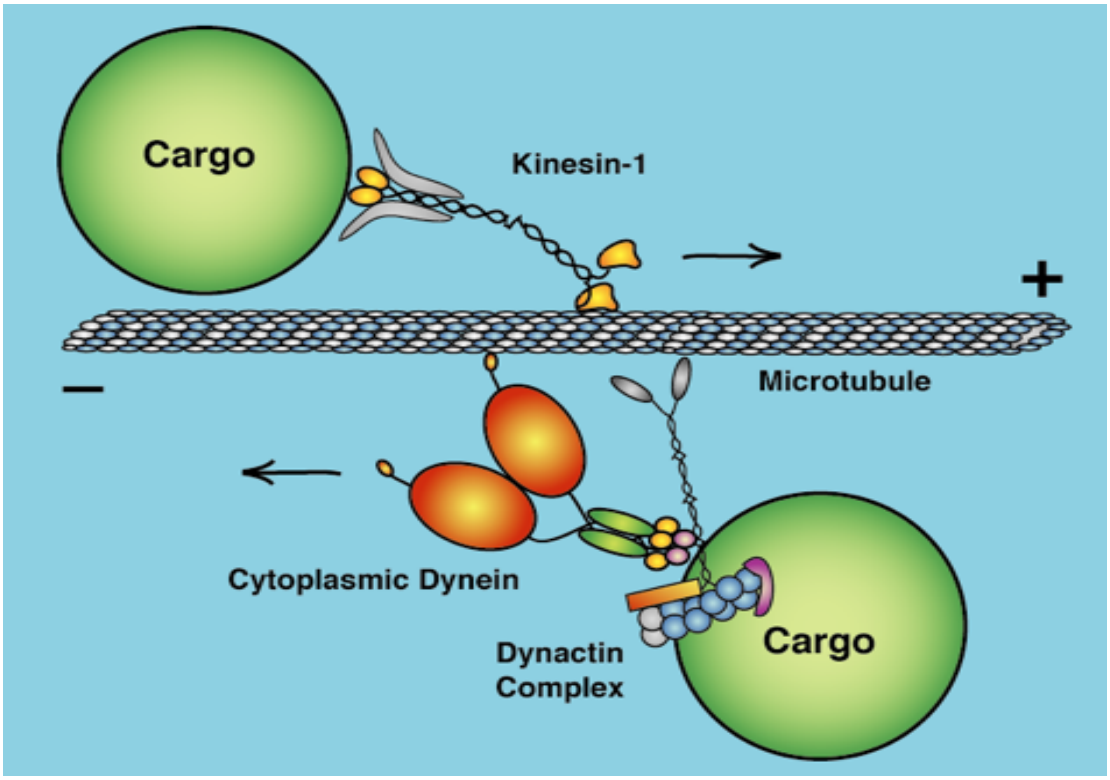

Figure 1.1. A microtubule with Kinesin-1 and Dynein. The microtubule is made up of alpha and beta dimers, represented in the figure as white and blue ovals, respectively. Kinesin-1, pictured here with Kinesin light chain in grey and bound to a green cargo, moves towards the plus end. Dynein, shown here with the Dynactin complex and a green cargo, moves towards the minus end of the microtubule.

has three major domains: the head domain, the neck linker, and the tail domain. The head domain binds to microtubules and to ATP, while the neck allows the flexibility needed for the hand-over-hand movement, and contains binding sites for linker proteins such as kinesin light chain (Klc) which bind the kinesin to its cargo (Vale and Fletterick 1997). The tail domain is important for motor regulation (Cai, Hoppe et al. 2007); (Coy, Hancock et al. 1999); (Dietrich, Sindelar et al. 2008). See Figure 1.1 for details.

Oogenesis in Drosophila melanogaster

The *Drosophila melanogaster* female has two ovaries, each consisting of around 18 ovarioles. Each of these ovarioles contains at the anterior end a germarium and a vitellarium at the posterior end, where later stages of oogenesis take place (King 1970) (Figure 1.2). The germarium contains somatic pre-follicle cells, germline stem cells, and early germ cell-follicle cell cysts. The stem cell divides asymmetrically to produce another stem cell and a cystoblast, which matures as it proceeds to the posterior end of the ovariole until it is a fully developed, fertilizable egg (Bastock and St. Johnston 2008). The cystoblast divides incompletely four times, giving rise to 16 cells, termed cystocytes, that remain connected by intercellular cytoplasmic bridges, or ring canals (Brown and King 1964) (Figure 1.3). The ring canals are surrounded by rings of F-actin (Warn, Gutzeit et al. 1985). The geometry of the cell divisions in the cystoblast depends on a structure of continuous endoplasmic reticulum called the fusome that connects through the ring canals and forms along the remnants of the

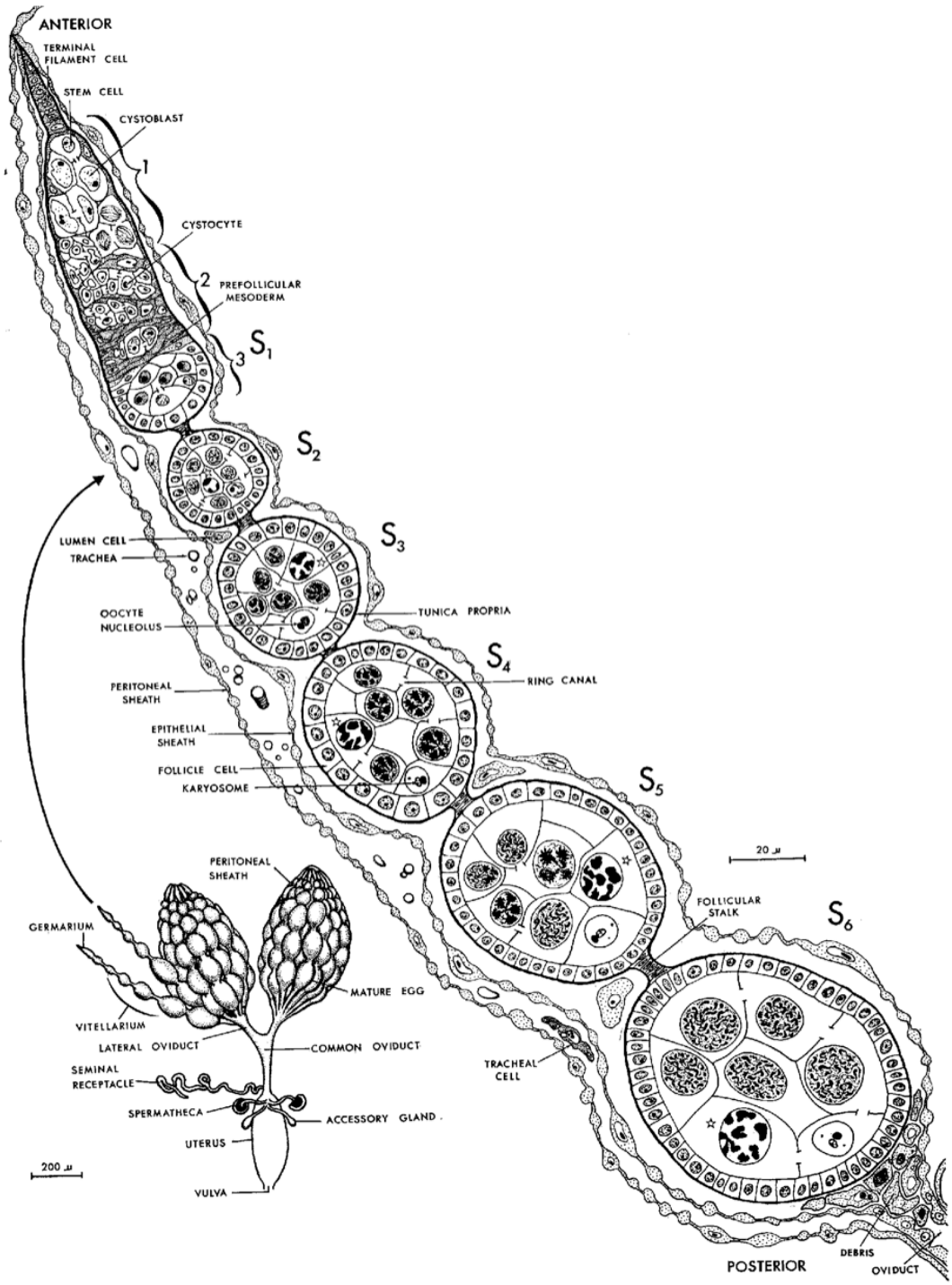
ANTERIOR
TERMINAL FILAMENT CELL
STEM CELL
CYSTOBLAST
1
CYSTOCYTE
2
PREFOLLICULAR MESODERM
3
S1
S2
S3
S4
S5
S6
LUMEN CELL
TRACHEA
OOCYTE NUCLEOLUS
TUNICA PROPRIA
RING CANAL
PERITONEAL SHEATH
EPITHELIAL SHEATH
FOLLICLE CELL
KARYOSOME
20 μ
FOLLICULAR STALK
PERITONEAL SHEATH
GERMARIUM
MATURE EGG
VITELLARIUM
LATERAL OVIDUCT
COMMON OVIDUCT
SEMINAL RECEPTACLE
SPERMATHECA
ACCESSORY GLAND
UTERUS
200 μ
VULVA
TRACHEAL CELL
DEBRIS
POSTERIOR
OVIDUCT

Figure 1.2. Ovariole and oogenesis through stage 6. In the lower left side of the figure, the reproductive track is shown with both ovaries and one ovariole separated from the rest to show the germarium and vitellarium. The germarium is pictured at the top of the figure, and the progression of oocyte development up until stage 6 is pictured from left to right. The oocyte is marked with a star in each of the egg chambers. (Image from (Cummings and King 1969)).

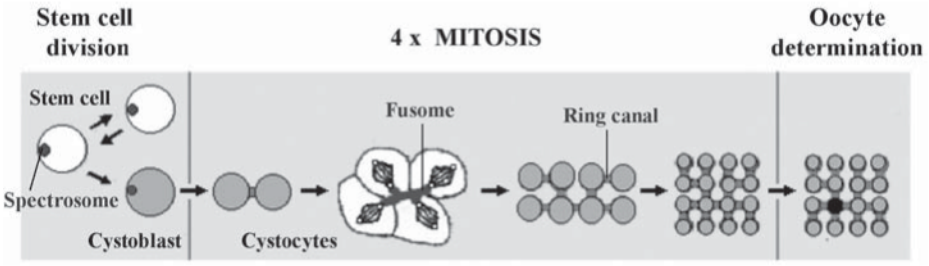

Figure 1.3 Cystoblast and cytocyte division and development.
The fusome is indicated in this figure, as are the ring canals and the incomplete division of the cytocysts. Ring canals connect the cytocysts. One of the cells from the initial division will become the oocyte, as indicated in the rightmost panel of the figure. (Image from (Máthé 2004))

mitotic spindle (Storto and King 1989); (Lin, Yue et al. 1994). The two cells from the first division are called pro-oocytes and contain 4 ring canals. Cell fate markers and meiotic chromosome pairing markers are restricted to these pro-oocytes. By the time the cystoblast is surrounded by somatic cells, these determinants are restricted to one cell that will become the oocyte; the other 15 cells become nurse cells (Figure 1.3) (Bastock and St. Johnston 2008). Microtubule inhibitor studies have shown that the localization of these determinants relies on microtubules to move into the oocyte (Theurkauf, Alberts et al. 1993). Posterior ring canals associated with the oocyte are largest, while ones further from the oocyte are smaller (Theurkauf, Smiley et al. 1992). Follicle cells begin to surround the cystocytes while the cluster remains in the germarium. Once a full complement of follicle cells has surrounded the germ cell cyst, it pinches off from the germarium and begins its journey down the ovariole. The cystoblast and somatic cell complex is referred to as the egg chamber. Oogenesis has been divided into 14 stages, dependent on egg morphology (Cummings and King 1969). The forming egg chamber, while still in the germarium, is said to be in Stage 1; once the egg chamber pinches off from the germarium, it enters Stage 2 (Figure 1.2).

Early Oogenesis

During stages 2-6 of oogenesis, nurse cells become polyploid and are highly transcriptionally active, while the oocyte is transcriptionally inactive and goes through meiotic prophase (King and Burnett 1959). The egg chamber remains

roughly spherical as it grows larger, with the oocyte growing at about the same rate as the nurse cells (Cooley and Theurkauf 1994). Oocyte growth is dependent on nutrients synthesized in and transported from nurse cells (Koch and Spitzer 1983). Throughout this period of oogenesis, microtubules emanate from an MTOC in the oocyte through the ring canals and throughout the 16-cell syncytium; this MTOC forms in stage 1 and is required for oocyte differentiation (Theurkauf, Alberts et al. 1993); (Koch and Spitzer 1983). This MTOC moves to the posterior end of the oocyte in Stages 2-6 (Theurkauf, Smiley et al. 1992).

Mid-Oogenesis

During stage 7, the follicle cells surrounding the oocyte become columnar, while those surrounding the nurse cells remain cuboidal (Cummings and King 1969). This same stage sees the oocyte beginning to endocytose yolk nutrients synthesized in fat bodies and the follicle cells surrounding it, which causes the oocyte to grow faster than the nurse cells (Cooley and Theurkauf 1994). By stage 10a, the oocyte comprises fully one half of the egg chamber (King 1970). During stage 7, lipid droplets begin to form in the nurse cells and are transported into the oocyte (Cummings and King 1969). The posterior MTOC degenerates in stages 7 and 8, and microtubule nucleating centers instead become associated with the anterior end of the oocyte, and by stage 9 an anterior to posterior gradient of microtubules has formed. The microtubules extend their plus-ends inward, forming a dynamic 3-D meshwork (Serbus, Cha et al. 2005); (Parton, Hamilton et al. 2011); (Theurkauf, Smiley et al.

1992), and are necessary for transporting the morphogenetic determinants that are localized throughout the oocyte during this period of oogenesis (Wang and Hazelrigg 1994); (Pokrywka and Stephenson 1991); (Clark, Giniger et al. 1994). *Bicoid* mRNA, an anterior morphogen, is localized to the anterior end of the oocyte (Berleth, Burri et al. 1988) while *oskar* is localized to the posterior (St. Johnston, Beuchle et al. 1991) and *gurken* accumulates between the oocyte nucleus and the dorsal cortex of the oocyte (Neuman-Silberberg and Schüpbach 1993) (Figure 1.4). These morphogens are anchored to the cortex so they are not disrupted during the next stages of oogenesis (for a review of this, see (Kugler and Lasko 2009)). During this same period of oogenesis, a small group of follicle cells called border cells begins migrating from the anterior end of the egg chamber by squeezing through the nurse cells to its eventual destination at the anterior end of the oocyte, adjacent to the oocyte nucleus (Figure 1.4). During stage 9, the follicle cells surrounding the oocyte begin secreting vitelline membrane, and during stage 10b, the anterior columnar follicle cells begin an inward centripetal migration until they meet with the border cells, enclosing the oocyte in follicle cells. By this stage, the oocyte is entirely surrounded by vitelline membrane, aside from the 4 ring canals, which remain until the nurse cells have completely regressed (Cummings and King 1969).

Late Oogenesis

Between stage 10b and stage 12, the microtubule cytoskeleton undergoes a massive rearrangement, forming parallel arrays below the oocyte cortex

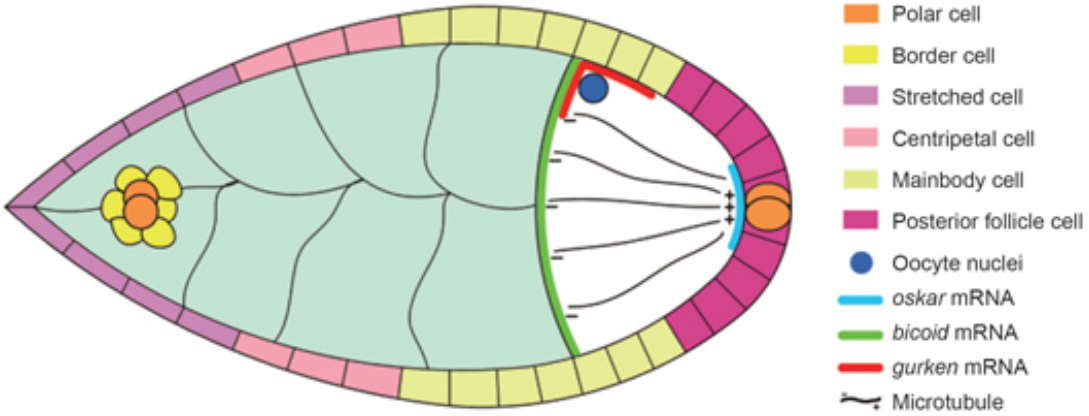

Figure 1.4 Mid-oogenesis egg chamber. The position of determinants is indicated by colored lines within the oocyte. The migrating border cells are shown as they begin traveling towards the oocyte to form the anterior follicle cells. (Image from (Li, Xin et al. 2007)).

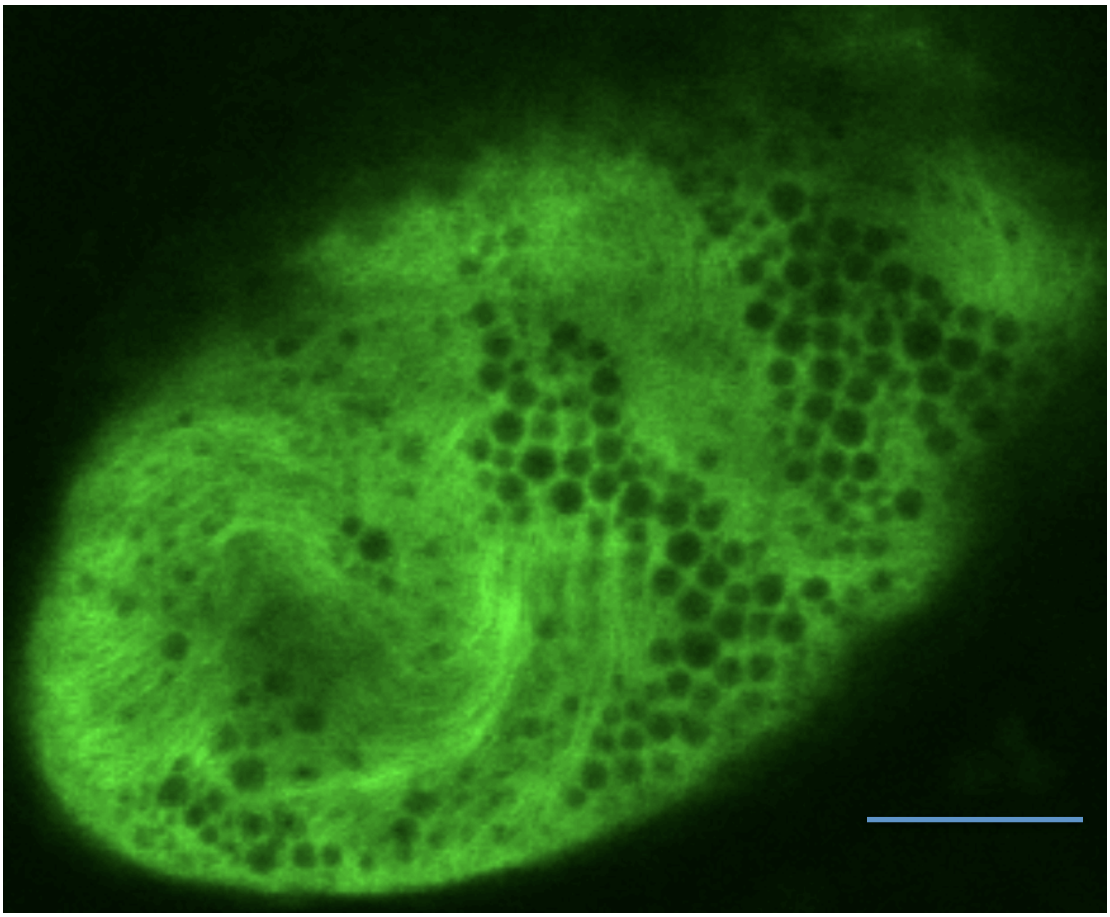

Figure 1.5 Stage 10B streaming oocyte expressing GFP-tubulin. Microtubules form parallel arrays just below the cortex. The black circles are yolk endosomes, some of which are streaming with the cytoplasm and others of which are caught above the microtubules against the cortex. Blue bar is 30 μm.

(Theurkauf, Smiley et al. 1992) (Figure 1.5). Once this rearrangement happens, the ooplasm begins a global, long-range movement called cytoplasmic streaming (Gutzeit and Koppa 1982).

During these stages, the nurse cells transfer all of their cytoplasm to the oocyte in a process known as dumping. As this occurs the oocyte doubles its size and the nurse cells completely regress (Mahajan-Miklos and Cooley 1994). Once the nurse cells have completely regressed, the subcortical microtubule arrays depolymerize and the meiotic spindle forms (Theurkauf and Hawley 1992). When dumping begins, the nurse cell nuclei become permeable and the karyoplasm is permitted to flow into the oocyte as well; however, the membranes and chromatin are retained in nurse cells (Cooley, Verheyen et al. 1992). Cytoplasmic actin networks form around the nurse cell nuclei (Gutzeit 1986). In mutants that do not permit this actin mesh to form, the nuclei get stuck in the ring canals like a cork in a bottle, and nurse cell cytoplasm is not allowed to flow into the oocyte. This results in small, infertile eggs (Cooley and Theurkauf 1994). The oocyte mixes the influx of nurse cell cytoplasm with its own ooplasm through cytoplasmic streaming, a microtubule and Kinesin-1 dependent process. Streaming gradually slows down in stage 12 as the bulk of cytoplasm has already been transferred in earlier stages. Once the nurse cells have completely emptied into the oocyte, streaming stops at the beginning of stage 13. In stages 13 and 14, the meiotic spindle assembles and the cell remains in metaphase of meiosis I until fertilization and egg activation begins (Cooley and Theurkauf 1994).

Cytoplasmic Streaming in Drosophila Oogenesis

Cytoplasmic streaming in *Drosophila* oocytes was first observed when it was discovered that oocytes could survive for long periods in Robb's medium *in vitro* (Robb 1969), and so time-lapse movies could be taken of the oocytes to record cytoplasmic behavior (Gutzeit and Koppa 1982). Streaming occurs in two stages: the first, termed slow cytoplasmic streaming, can be seen between stages 7-10a, and involves disordered oscillatory movements that occur in the anterior of the oocyte (Theurkauf 1994); (Serbus, Cha et al. 2005). This process aids in the targeted localization of polarity determinants *bicoid, oskar, and gurken* to their respective locations in the anterior, posterior, and dorsal areas of the developing oocytes, which establish the major body axes of the future organism (Ephrussi and Lehmann 1992); (Berleth, Burri et al. 1988); (Kim-Ha, Smith et al. 1991); (Riechmann and Ephrussi 2001) (Figure 1.4). Kinesin-1 is abundant and diffusely distributed with elevated concentrations around the cortex and at the posterior (Palacios and St. Johnston 2002); (Brendza, Serbus et al. 2002), and the paths of slow cytoplasmic flows are short and randomly directed (Figure 1.6 A and B, left side). The second, termed fast cytoplasmic streaming, occurs between stages 10b and 13, and involves long-range ordered movements of cytoplasm throughout the whole oocyte (Serbus, Cha et al. 2005) (Figure 1.6 A and B, right side). At the beginning of stage 10B, ooplasm begins to engage in fast cytoplasmic streaming, but nurse cell cytoplasm has not yet begun to dump into the oocytes (Gutzeit and Koppa 1982). Shortly after, nurse cells begin dumping their cytoplasm into the anterior end of the oocyte, beginning with the nurse

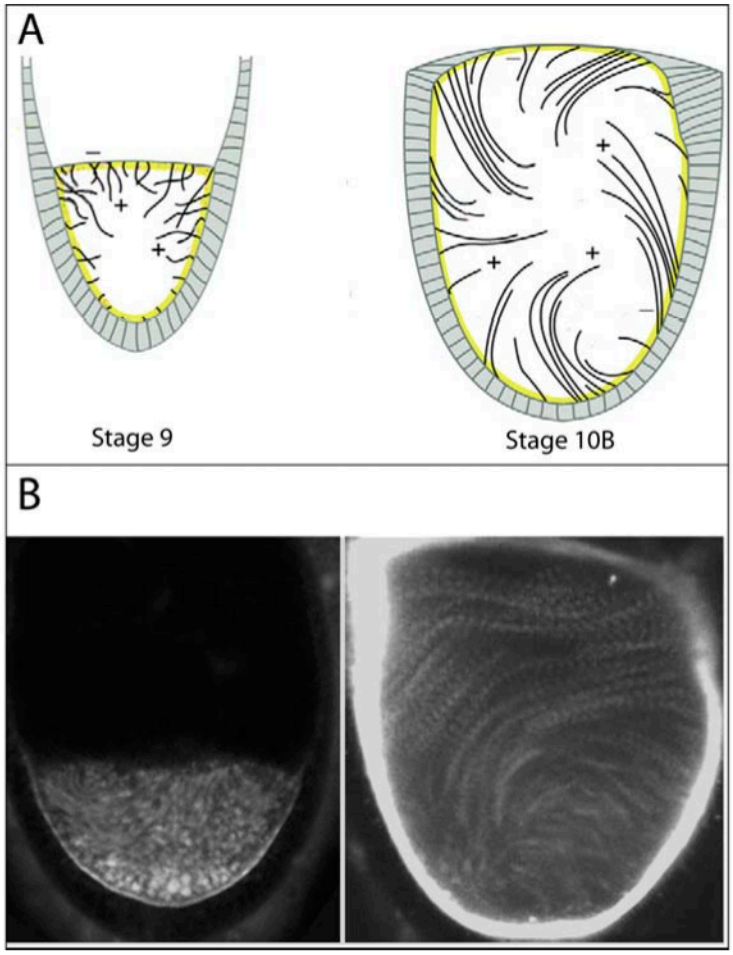

Figure 1.6 Microtubule organization and streaming in the *Drosophila* oocyte. A) Schematic of the change in microtubule organization in stage 9 and 10b oocytes. Minus ends are shown embedded in the actin-rich cortex (yellow) and plus ends are shown free in the cytoplasm (Image adapted from Serbus *et al.*, 2005). B) Time-lapse projections of movies from slow and fast streaming oocytes. Streaks represent yolk endosomes that are moving in the cytoplasmic flow, while stationary endosomes appear as dots. A stage 9 oocyte showing slow streaming at the anterior where MTs are enriched (left). Fast streaming is distributed througout the whole oocyte during stage 10b until stage 13. (Image from (Moua 2009).)

cells adjacent to the oocyte (Cummings and King 1970). Gutzeit and Koppa conjectured that fast cytoplasmic streaming and dumping must be independent processes; fast streaming cannot be predicated by dumping as it begins before dumping does. Once all nurse cell cytoplasm has been transfered into the oocyte, cytoplasmic streaming begins to slow down, and microtubules begin forming shorter, denser bundles; the cortex at the anterior end also grows thicker, up to 15μm thick (Gutzeit and Koppa 1982). By stage 13, all cytoplasmic streaming has ceased.

Cytoskeleton and Motor Proteins in Cytoplasmic Streaming

Cytochalasin inhibits the movement of cytoplasm from the nurse cells, but ooplasmic streaming continues, implying that nurse cell dumping is an actin-controlled process but ooplasmic streaming is not (Gutzeit 1986). When oocytes are treated with colchicine, eggs do not develop (Koch and Spitzer 1983), and cytoplasmic streaming doesn't occur (Gutzeit 1986). The movement involved in streaming, then, is a microtubule-driven process. This is supported by the appearance at stage 10b of long, evenly distributed arrays of microtubules between 5 and 10 μm below the surface of and parallel to the oocyte cortex (Theurkauf, Smiley et al. 1992); (Serbus, Cha et al. 2005) (Figure 1.5).

Kinesin-1 was discovered to drive the movement behind cytoplasmic streaming in the *Drosophila* oocyte. Mutations in the head of kinesin and null *Khc* mutants stopped streaming entirely, both slow and fast streaming (Palacios and St. Johnston 2002). *Klc* null oocytes continue to stream, though they show a significantly reduced

rate of streaming, implying that Klc is not essential for this process, but may still have some influence (Moua 2009). *Khc* mutants show a stratification of ooplasm and nurse cell cytoplasm, which suggests that cytoplasmic streaming is necessary for mixing the two cytoplasms together (Serbus, Cha et al. 2005).

While Kinesin-1 drives cytoplasmic streaming, dynein also has an influence. When inhibitory dynein antibodies were injected into oocytes in the slow streaming stages, fast streaming started prematurely (Serbus, Cha et al. 2005). These data suggest that Kinesin-1 is important in both slow and fast streaming, but dynein is only active during slow streaming; there may be some endogenous dynein inhibition that takes effect at the beginning of stage 10b.

Although the actin cytoskeleton is not directly involved in force production in cytoplasmic streaming in *Drosophila*, it does influence the timing of streaming in a way similar to the role of dynein. Myosins do not seem to be involved in streaming, although Myosin II is involved in transport from the nurse cells to the oocyte (Wheatley, Kulkarni et al. 1995). However, when F-actin is disrupted by cytochalasin, premature fast streaming can be seen as early as stage 4 (Emmons, Phan et al. 1995), and mutations in actin regulators *cappuccino, spire,* and *chickadee* cause premature fast streaming (Dahlgaard, Raposo et al. 2007); (Magie, Meyer et al. 1999); (Manseau, Calley et al. 1996); (Otto, Raabe et al. 2000); (Verheyen and Cooley 1994); (Wellington, Emmons et al. 1999); (Theurkauf 1994). Over-expression of *spire* causes the actin meshwork to perdure beyond stage 10b, when it normally dissociates, which keeps fast streaming from occurring (Dahlgaard, Raposo et al.

2007). As a result of this premature fast streaming, *oskar* and *gurken* mRNA are mislocalized, likely due to not being anchored correctly to the cortex and being swept away by fast streaming (Manseau, Calley et al. 1996); (Manseau and Schüpbach 1989); (Wellington, Emmons et al. 1999). This mislocalization leads to polarity defects and embryo death, showing that the precise control and timing of the start of fast streaming is vital to the survival of the organism. The transition from slow disordered to fast-ordered streaming coincides with a centripetal shift of cortical microtubule minus-end nucleation factors and with loss of a filamentous actin (f-actin) meshwork that permeates the ooplasm (Dahlgaard, Raposo et al. 2007); (Wang and Riechmann 2008). It is particularly interesting that cytoplasmic f-actin depolymerization can trigger premature microtubule alignment and fast streaming in mid oogenesis (Theurkauf 1994); (Dahlgaard, Raposo et al. 2007). These and other observations suggest that microtubule disorder and slow streaming reflect plus-end directed kinesin-1 motion that, although capable of organizing microtubules and fast fluid flows, is somehow opposed by microtubules disorder and a cytoplasmic f-actin meshwork. Unknown signals at the beginning of stage 10B allow a kinesin-1 dominated self-amplifying loop of microtubule alignment and fast plus-end directed fluid motion that mixes oocyte and nurse cell cytoplasm (Serbus, Cha et al. 2005); (Dahlgaard, Raposo et al. 2007).

To gain insight into kinesin-driven microtubule alignment and fluid flows, we used confocal fluorescence microscopy of live oocytes to examine spatial and dynamic relationships between the oocyte boundary, microtubule behavior, and

cytoplasmic motion. We then used basic physical principles to develop a detailed mathematical model for the streaming mechanism. Starting with known values for kinesin-1 velocity on microtubules and an estimate of cytoplasmic viscosity, the model explores kinesin cargo size/spacing relationships that could generate enough viscous drag to drive the observed velocity of fast streaming. This leads to an interesting conclusion that the naked motor without any organelle cargo could drive the observed fast ooplasmic flows. The model then focuses on the influence of kinesin-like force on a filament with the stiffness of a microtubule whose minus end is tethered in an unbounded cytoplasmic flow field. Starting from any configuration, a random filament bending pattern evolves into a stable helical wave. To examine a complex situation more similar to that of an oocyte, we coupled the models for cytoplasmic flow generation and filament bending to test a field of many filaments with minus ends held tethered to a cortex-like barrier plane. Simulations showed filament behaviors ranging from a largely disordered bending state to a remarkably ordered state with aligned bending arrays that lay parallel to the cortical plane. A key factor for evolution of the ordered state is the distance between the cortical barrier and the level at which filaments can become parallel to it. The other important variables were those that influenced bending; filament stiffness and the determinants of motor force density on them, notably including cytoplasmic viscosity.

Chapter Two

Kinesin-driven self organization of microtubules and fast cytoplasmic streaming: A mechanism for mixing fluid at low Reynolds number.

Introduction

Transport processes that purposefully move organelles, chromosomes, and other objects from one place to another are fundamental to the reproduction, growth, and development of eukaryotic cells. A great deal is known about how molecular motors generate processive stepping forces that move objects along directional cytoskeletal filaments. Motors couple cycles of ATP-driven motor conformation change to cycles of filament binding and release that advance in one direction along the filament (Vale and Milligan 2000). Less attention has been paid to the influences of motor generated forces on the filament tracks and on the cytoplasmic fluid through which motors and their cargoes move. We report here analysis of a transport process in the *Drosophila* oocyte that offers unique insights into how filament and fluid responses can have profound long-range influences on cytoplasmic organization. Our results shed light on the hydrodynamic underpinnings of transport processes, they elucidate a general and hitherto unknown form of filament self organization, and they point out a novel mechanism for mixing fluid at low Reynolds number, which is a problem that has been difficult to solve.

In the *Drosophila* ovary, a germline stem cell generates an egg chamber with 15 nurse cells that are connected by cytoplasmic channels to one another and to the

anterior end of a new oocyte. During the early and mid stages of oogenesis, mRNAs, protein complexes and organelles that are synthesized in nurse cells are selectively transported into the oocyte (Cooley and Theurkauf 1994). Slow disordered cytoplasmic flows help disperse the new components after they enter the oocyte anterior. During this period, developmental determinants, such as *bicoid* and *oskar* mRNAs, are concentrated in particular regions of the oocyte cortex and anchored, thereby establishing the major body axes of the future organism (Ephrussi and Lehmann 1992); (Berleth, Burri et al. 1988); (Kim-Ha, Smith et al. 1991); (Riechmann and Ephrussi 2001). Substantial amounts of other materials synthesized in somatic tissues, such as yolk granules, are transferred into the developing oocyte through its lateral and posterior walls by endocytosis. In late oogenesis, at the beginning of stage 10B, nurse cells transfer all their remaining cytoplasm into the oocyte anterior *en masse*. To mix this new material with the existing yolky ooplasm, the slow disordered flows convert to massive fast flows that follow long, curving paths throughout the oocyte (Gutzeit and Koppa 1982). Mutations that allow premature fast streaming during mid oogenesis prevent proper anchoring of molecular determinants to the cortex and thus disrupt the development of body axis polarity (Theurkauf 1994). Mutations that allow no fast streaming prevent the mixing of oocyte with nurse cell cytoplasm and cause embryonic lethality (Brendza, Serbus et al. 2000); (Palacios and St. Johnston 2002); (Serbus, Cha et al. 2005). Therefore, the mechanisms that control the transition from slow to fast streaming are crucial.

Results

Streaming flows and microtubule bending.

To gain insight into the behaviors of microtubules and cytoplasm during streaming, we used time-lapse fluorescence microscopy to image living oocytes dissected from females that expressed GFP-tubulin specifically in their germlines (Figure 2.1, and Movies S1-3). Comparison of stage 9 (slow streaming) and 10B (fast streaming) oocytes revealed striking differences. Fibrous fluorescence from microtubules in stage 9 was diffuse and exhibited a disordered writhing behavior, with yolk particle motions that were disordered, slow, and accomplished little net displacement over time (Figure 2.1A, B, and Movie S1). This pattern did not vary substantially at different depths beneath the oocyte surface. In stage 10B near the oocyte margin, microtubule fluorescence was diffuse amongst a layer of yolk granules that moved slowly if at all, presumably constrained by association with the cortex (Fig. 2.1C, D, lower left, and Movie S2). Further in, about 5um beneath the plasma membrane, and parallel to it, there was a thin dense zone of aligned microtubules that exhibited remarkable wave-like bending behaviors. Yolk granules just beneath that layer moved fast over long distances, generally following the paths of the nearby microtubule arrays. These observations suggest important biophysical relationships between distance from the oocyte surface, microtubule ordering, and cytoplasmic flow velocity during stage 10B that are not present in the earlier slow streaming stages of oogenesis.

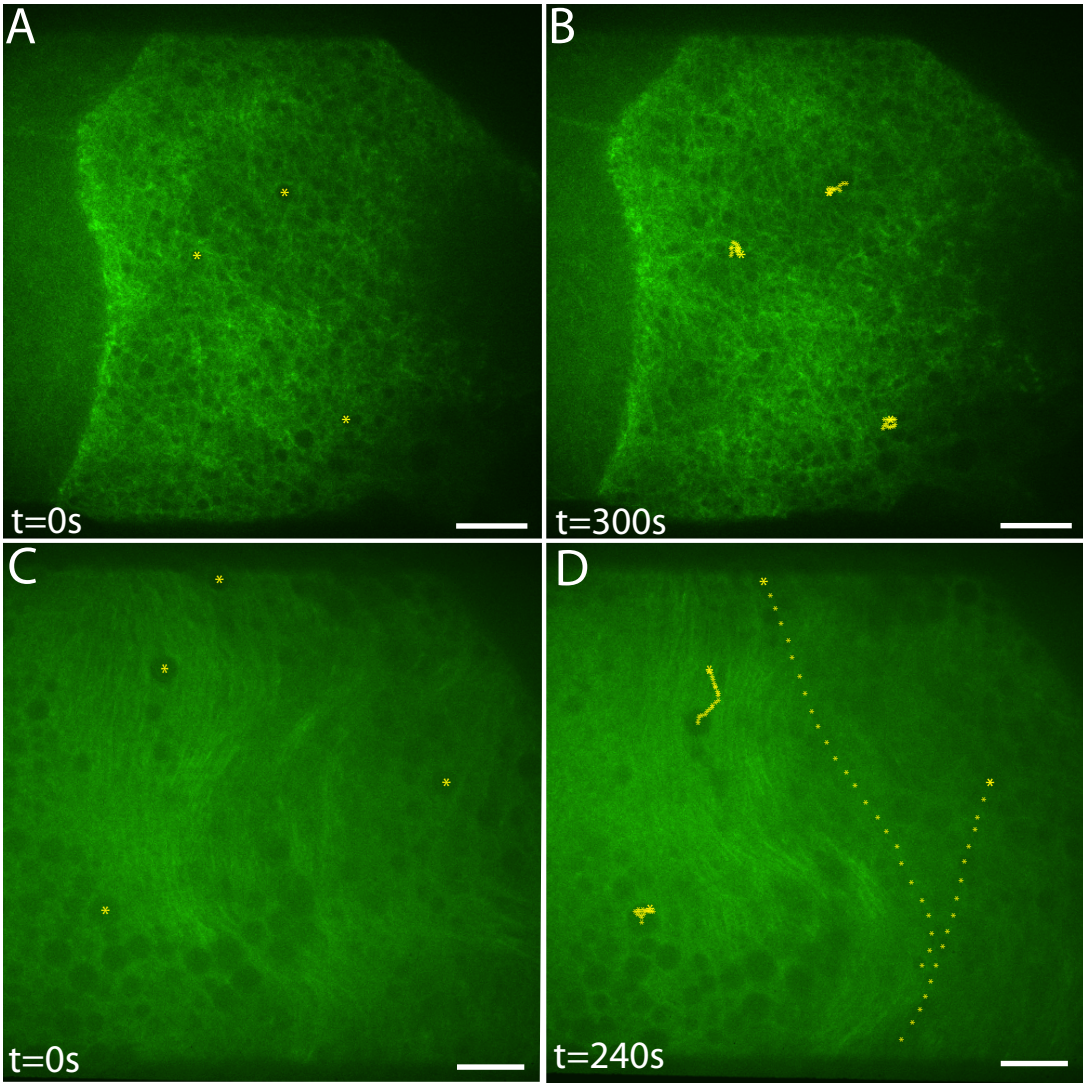

Figure 2.1 Microtubule organization and yolk granule motion in *Drosophila* oocytes. Single optical sections from beneath the plasma membrane of live oocytes that contained GFP-a-tubulin. A) A stage 9 oocyte with the centers of three yolk granules marked by yellow dots. B) The same oocyte 5min later with the positions of the three yolk granules marked at intervening 10sec intervals. The optical section is near the surface of the oocyte at the right side and is ~10µm beneath the surface at the left side. Note the similarly disordered microtubules and slow granule movements at all depths. C) and D) A stage 10B oocyte with granules marked and tracked as in A and B. In this case, the optical section is just beneath the oocyte surface at the lower left and is ~10µm deeper on the right. Note the thin layer of parallel microtubules at ~5µm depth. Organelle motion was slow between the microtubule layer and the oocyte surface (left side), and was fast just beneath the microtubule layer (right side). Only yolk endosomes that remained in the focal plane were used to mark streaming motions in this figure. Similar oocytes can be observed in Movies S1-S3. Scale bars = 10µm.

Microtubule minus ends are tethered to the cortex.

One of the key assumptions for oocyte cytoskeleton organization is that many microtubule minus-ends are tethered in or near the oocyte cortex (Theurkauf, Smiley et al. 1992). During slow streaming stages, gamma-tubulin, which nucleates α β tubulin polymerization and binds minus-ends, is concentrated in the dense f-actin network of the oocyte cortex (Wang and Riechmann 2008); (Cha, Serbus et al. 2002). Microtubule polymerization begins in or near the cortex with tubulin dimers adding to the plus-ends, which extend toward the center of the oocyte or generally away from the cortex (Theurkauf, Smiley et al. 1992); (Parton, Hamilton et al. 2011); (Cha, Serbus et al. 2002). However, the change from slow disordered to fast ordered streaming correlates with a shift of gamma-tubulin inward to a more diffuse distribution, suggesting that microtubule minus-ends could be freed from cortical anchors at the beginning of fast streaming (Wang and Riechmann 2008).

If microtubules are not tethered to the cortex during fast streaming, they should be carried along in the cytoplasmic flow. To test this, we analyzed GFP-tubulin dynamics by fluorescence redistribution after photobleaching (FRAP) in stage 10B oocytes using a two-photon microscope. Well aligned subcortical microtubules were marked by photobleaching then the positions of the bleached zone and of streaming yolk granules were subsequently followed by time-lapse imaging (Figure 2.2, Movie S4). If minus-ends were not tethered and microtubules were thus free, the bleached mark should move along with yolk granules in the cytoplasmic flow.

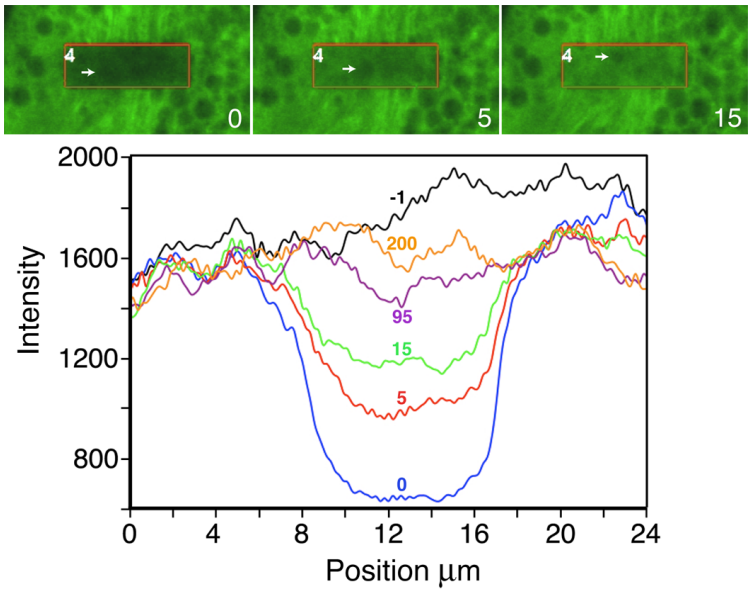

Figure 2.2 Subcortical arrays of microtubules are stationary during streaming. Top: GFP-tubulin in a stage 10B oocyte imaged by time-lapse two-photon fluorescence microscopy. Intense 2-photon excitation was used to photobleach a 10x 30µm area (orange box) in well aligned subcortical microtubules. White arrows mark the positions of a yolk granule carried by fast streaming at 0.3µm/sec. Bottom: Fluorescence intensity was scanned from bottom (0µm) to top (24µm) of images at various time points (noted in seconds). The bleached zone did not move laterally and fluorescence recovery was symmetrical, despite streaming of cytoplasm through the area (see Movie S4).

The bleached zones recovered fluorescence rapidly over the course of approximately one minute, but their recovery was symmetrical and they made no discernible shifts in position, despite fast flow of yolk granules through the zones. This shows that aligned arrays of subcortical microtubules are not carried along by cytoplasmic streaming flows, indicating that minus-ends are indeed tethered to the stage 10B cortex.

In order to further test this, we observed streaming in flies expressing the photoconvertible fluorescent protein Dendra fused to tubulin monomers in oocytes. Using the MOSAIC system to expose a small selected area of subcortical microtubules to blue light for 6 seconds caused the exposed protein to go from fluorescing green to fluorescing red. If microtubules were anchored to the cortex, we would expect to see a number of red microtubules remain in the area and not move with the direction of flow. In our movies, a number of red microtubules remain in place for the duration of the movie, despite what may be free tubulin moving in the direction of flow (Figure 2.3, Movie S8). This provides further evidence that microtubules are tethered to the cortex.

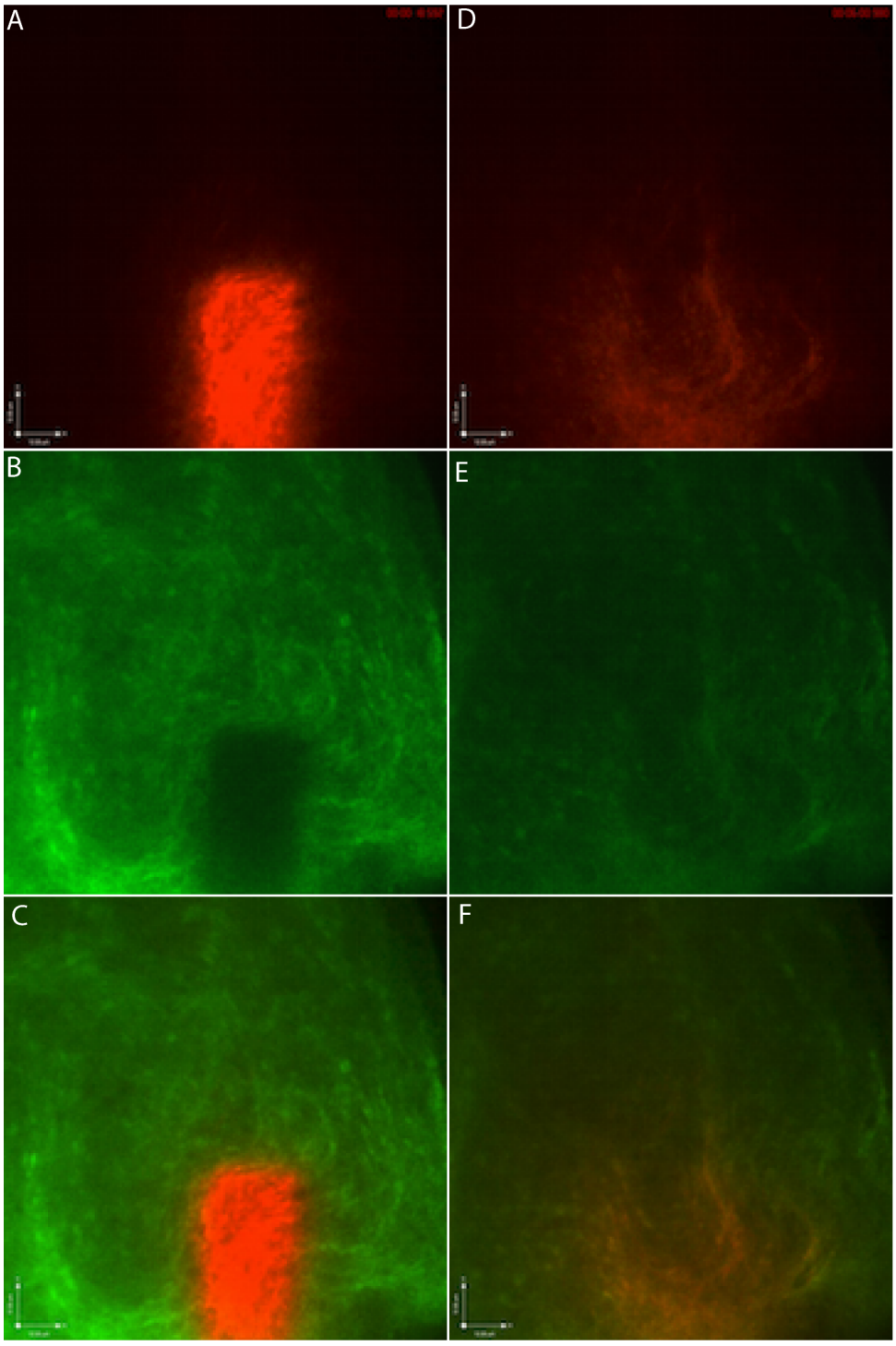
A
D
B
E
C
F

Figure 2.3 Subcortical microtubules are stationary during streaming.
Photoconvertible Dendra2-tubulin protein expressed in Stage 10b oocytes time-lapse imaged with confocal microscopy. A-C: 18 seconds, immediately post-conversion with blue light. A. is the red channel, B. the green, and C. is the two colors merged. D-F: 360 seconds, D. is the red channel, E. is the green channel, and F. is the two merged. Area converted is approximately 24μm wide and 40μm tall. Microtubules converted from green to red remain in the same area and do not travel with the cytoplasmic flow. General direction of flow is in a broad clockwise horseshoe beginning at the top right of the image. Scale bar is 12 μm.

A mechanism for kinesin-driven fluid flow and microtubule bending

Our findings, joined with past observations cited above, support a mechanism for fast streaming that is unique in its simplicity, relying primarily on a single filament type, microtubules, and a single motor protein species, kinesin-1. At the beginning of stage 10B, changes occur that allow robust movement of kinesin-1 along microtubules whose minus-ends are tethered to the cortex. The kinesin-1 motors and their organelle cargoes transfer force to adjacent cytoplasmic fluid by viscous drag and hence cytoplasm moves toward plus-ends. The force of each kinesin-1 on fluid is matched by an equal and opposite force on its microtubule that would displace it with the minus-end leading, if it were free to move. However, because its minus-end is tethered to the cortex, the microtubule responds to the kinesin force by bending. In the fast streaming state, hydrodynamic force transfer between neighboring microtubules, combined with drag on them from cytoplasmic flow toward their plus-ends, encourages parallel alignment and a correlation of bending behaviors. The correlated bending patterns change over time, creating directions for fluid flows whose continuous variation facilitates non-laminar and thus efficient mixing of cytoplasm, despite its high viscosity and the small scale of the process.

Fluid flow caused by kinesin-driven motion

To elucidate the proposed mechanism in quantitative terms, we considered three lines of inquiry: 1) How can bulk cytoplasmic fluid flows be driven by the movement of kinesin motors toward microtubule plus-ends? 2) How does

microtubule bending occur in this situation? and 3) How can the combination of these two effects lead to a self organizing system of fast flows, aligned microtubules, and correlated bending behavior? To address these questions, a mathematical model was developed based on the physical principles of hydrodynamics. Simulations of the model were used to determine if it can explain the disordered and the aligned phases and, if so, what the key parameters are for self-organization.

We first developed a physical model for fluid flows based on known properties of microtubules, kinesin-1, and cytoplasm. A small moving object will interact with its surrounding cytoplasm by viscous drag (Berg 1983); (Purcell 1977), moving the fluid such that flow velocity decreases with distance away from the object, r, as $1/r$. Thus, a single kinesin-cargo complex traveling along a microtubule can move neighboring fluid, but the velocity of that movement becomes negligible at large distances. However, as illustrated in Figure 2.4, a linear array of spherical objects (*e.g.* kinesin-cargos) of diameter a, moving at velocity v_0, that are separated by distances of d, will create drag similar to that of a long rod. For distance scales $>>$ d, this train of objects is equivalent to a solid rod of diameter a, moving at a velocity of approximately $(a/d)\ v_0$. A moving rod generates a flow field with velocities that can be substantial at large distances. In fact, the effect of a moving rod of length L is similar to the effect of a moving sphere of diameter L, up to slowly varying logarithmic corrections (Berg 1983). Thus, fluid velocity will be comparable to the velocity of the rod out to distances of order L. With kinesin-cargo complexes

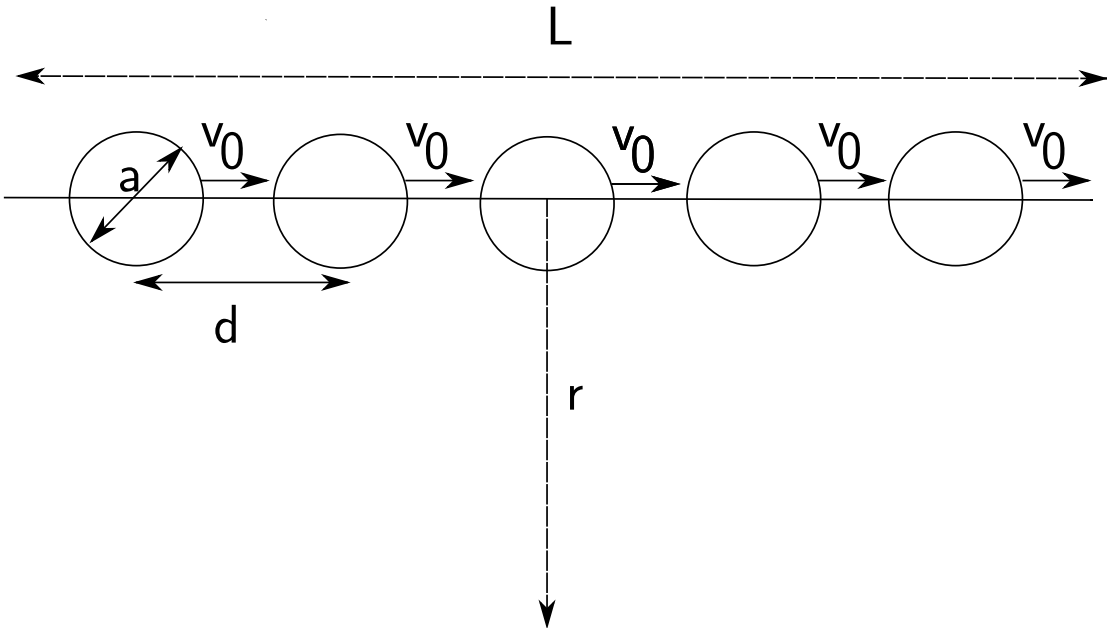

Figure 2.4. Fluid movement by viscous drag on a train of impellers at low Reynolds number. A train of spherically shaped impellers of diameter *a* and separation *d*, all moving in a fluid with low Reynolds number at velocity v_0. The fluid velocity v*(r)* is measured at a point distance *r* from the axis. Separated by small distances, these impellers should behave as a rod of length *L*.

closely spaced all along a microtubule, L will be equivalent to the length of the microtubule, which in an oocyte could average tens of microns.

This analysis leaves out the effect of the oocyte cortex, which will inhibit fluid flow next to its surface. To analyze this situation, as with the many aligned microtubules that are in the subcortical layer during fast streaming, we considered an infinite array of parallel rods lying above a wall (Figure 2.5). Here each rod is moving along its length causing viscous drag and thus hydrodynamic flow into or out of the page. The cortex-like barrier below it maintains a velocity of zero (dark blue) at its surface. The hydrodynamics of this situation can be understood by electrostatic analogy because it maps onto the problem of an array of rods at constant potential above a grounded plane, and can be solved by the method of images. In this case, fluid far from the wall and the rods moves at a constant intermediate velocity (green in Figure 2.5). Therefore, a two dimensional layer of microtubules above the cortex with closely spaced kinesin cargoes moving along their surfaces could cause mass fluid flow in an oocyte.

Now we are in a position to determine the relationship between the velocity of kinesin and that of ooplasm during fast streaming. The velocity of ooplasm should be less than that of kinesin moving on cortical microtubules by the factor of approximately a/d. Kinesin-1 driven motions in metazoan cells vary from ~100 to 1000nm/s depending on which cargo type is being tracked, and perhaps on regulatory

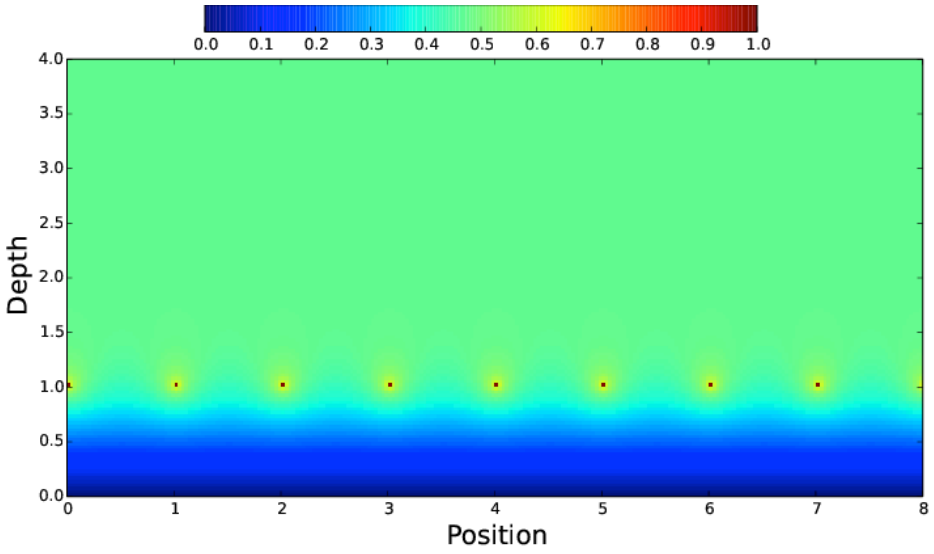

Figure 2.5. Model of a fluid flow velocity field generated by kinesin-like motion along microtubules. A cross-sectional view of an array of infinitely long microtubule-like rods (red dots) suspended in fluid at a depth of 1 (arbitrary) unit above a non-moving cortex-like barrier. Coated evenly with kinesin-cargo complexes moving at a constant velocity (1, red in scale bar), into or out of the page, each rod generates fluid flow in that same direction. Relative fluid velocities are represented by colors as shown above in the color bar, with red being equivalent to the kinesin velocity, yellow and green intermediate, and blue slow. Velocity is fastest around each microtubule, goes linearly to zero at the cortical barrier plane (y=0), and asymptotes to a constant intermediate value above the microtubule plane (green).

influences or how many kinesins are engaged in moving each cargo (Pilling, Horiuchi et al. 2006); (Zimyanin, Belaya et al. 2008); (Shubeita, Tran et al. 2008); (Kural, Kim et al. 2005).

We elected to use the velocity of kinesin-1 itself measured directly in cells at v_0 = 780nm/s (Cai, Hoppe et al. 2007). In our tests, the average velocity of fast streaming just beneath the microtubule layer is 217 +/- 38nm/s (n=12 oocytes), suggesting that a/d is 0.28. With an average cargo diameter of a = 250nm (*e.g.* lipid droplets), a spacing of d = 0.9μm along microtubules should be sufficient to support the observed streaming velocity. Electron microscopy has, in fact, shown that there can be close association between lipid droplets and subcortical microtubules in stage 10B oocytes (Theurkauf, Smiley et al. 1992). However, any kinesin-cargo complex should suffice if appropriately spaced along microtubules; *e.g.* 40nm diameter small vesicles would need to be spaced at 140nm. This logic leads to consideration of the possibility that kinesin-1 motors, each with its own rod-like geometry 30-80nm long (Amos 1987), could drive fast streaming with no cargo attached if they were closely spaced along microtubules. In summary, this fluid flow analysis indicates that kinesin forces that are transferred to surrounding cytoplasmic fluid by viscous drag can indeed explain the magnitude and velocity of fluid motion in fast streaming oocytes, even at substantial distances from the cortical microtubule layer.

Dynamics of kinesin-driven microtubule bending

Can kinesin forces explain the correlated wave-like bending motions of microtubules seen during fast streaming? The general logic we use to analyze this considers the multiple forces that act on cortical microtubules. One is the force kinesins exert directly on a microtubule; a force tangent to its long axis. This buckling force is resisted by the elastic stiffness of the microtubule. Another force is that which moving cytoplasmic fluid exerts on the microtubule. Thus, the analysis must incorporate the determinants of fluid motion, which begin with moving kinesin complexes, but also must include the motions and conformations of the microtubules. It is consideration of these coupled effects that allows one to evolve the entire hydrodynamic system in time.

First consider the magnitude of the force exerted by an individual kinesin motor on its point of attachment to a microtubule. This is equal and opposite to the viscous drag on the motor-cargo complex as it moves toward the plus-end. With a motor complex of linear dimension a, the force due to Stokes drag is $3\pi\eta a$v . Assuming a cytoplasmic viscosity η of 8 times that of water (Luby-Phelps 2000), and an *in vivo* kinesin velocity v of 780nm/s, the drag force from even a large cargo ($a = 2\mu$m) would be only 0.12pN, and from a small cargo, or just the motor itself (a= 60 nm) would be 0.007pN. The force per unit microtubule length, f_k, generated by a train of kinesin complexes walking along the microtubule can be estimated because it is proportional to η, v, and as discussed above, a/d, so that $f_k = \eta$va/d. This

force density is independent of microtubule length, up to logarithmic corrections, and the load on a kinesin due to drag is far less than its stall force (>5pN) (Svoboda and Block 1994).

We now use these observations to construct a model for the motion of a single minus-end tethered microtubule interacting with many kinesins in fluid. Consider the multiple forces that act at any point on the microtubule (Figure 2.6). As a kinesin steps toward the microtubule plus-end, it applies force to the surrounding fluid and it transfers an equal-opposite force ($\boldsymbol{F}_k$) to the microtubule that is tangent to its long axis. Assuming that the microtubule is inextensible, the force on the microtubule creates a tension T acting on nearby elements in opposing directions, giving a net force that we denote ΔT. The microtubule has an elastic bending constant C that will produce a force $\boldsymbol{F}_e$ perpendicular to the microtubule long axis. The total local force acting on an element of fluid next to a microtubule is the sum of the above forces,

$$\boldsymbol{f} = \boldsymbol{F}_e + \boldsymbol{F}_k + \Delta T \tag{1}$$

This equation, supplemented with more detailed expressions for the terms on the right hand side (described below), gives the force acting on a point in the fluid, but this is not enough to determine the motion of the system. Hydrodynamic theory can be used to obtain that motion: The total force acting on an element of liquid has a long-range influence on velocities far from that point. The velocity of the fluid due to a force

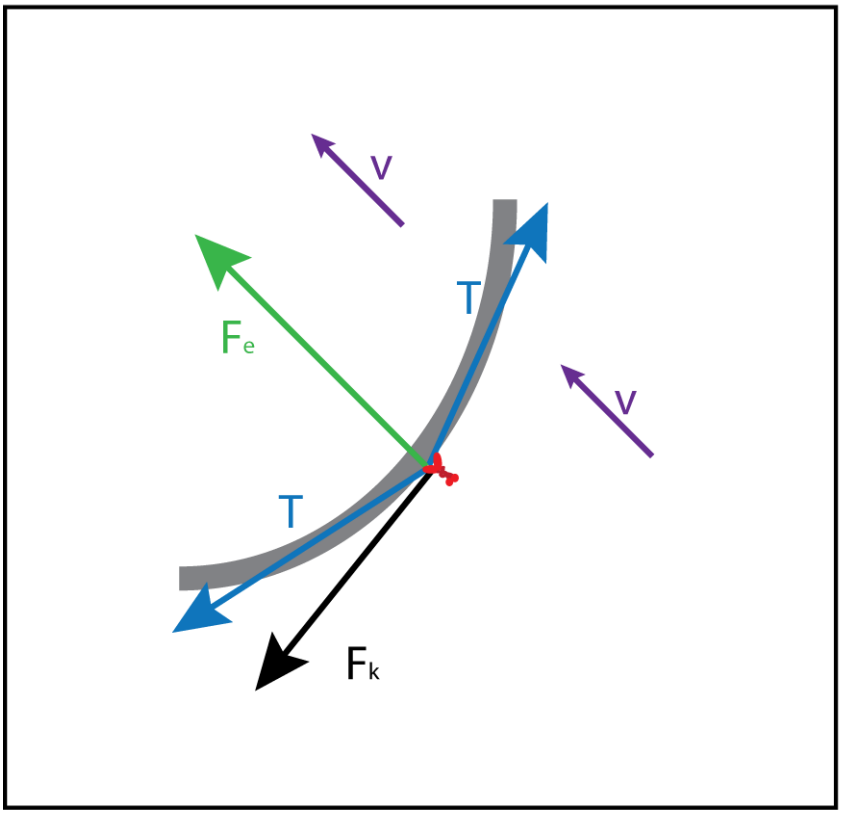

Figure 2.6. Force diagram for a microtubule-kinesin system. A small section of a microtubule (gray), is shown being acted on by kinesin forces all along its length that cause bending. A single kinesin (red) is shown to focus attention on multiple forces (arrows) that act at its point of attachment to the microtubule. A force tangent to the long axis of the microtubule is exerted by kinesins causing a total force in this section of $\boldsymbol{F}_k$. The microtubule has an elastic bending constant which will produce a force ($\boldsymbol{F}_e$) in this section, that will oppose the microtubule bending. Tension (T) acts on neighboring elements of the microtubule in opposing directions tangent to the long axis. Force transfers from the microtubule to surrounding fluid that moves at a velocity **v**.

acting on a point, is given by the Oseen tensor, which dictates that far from any surfaces, fluid velocity will diminish as the inverse of distance from the point of force, with an additional prefactor of order unity, depending on the force's direction. Conversely, the velocity $\mathbf{u}(\mathbf{r})$ of fluid at an arbitrary point $\mathbf{r}$, is the weighted sum over all forces. In more precise terms, this weight is the Oseen tensor $\mathbf{J}(\mathbf{r}, \mathbf{r}')$, which connects the force density $\mathbf{f}(\mathbf{r}')$ at point $\mathbf{r}'$ in the fluid to the velocity at another location, $\mathbf{r}$, so that

$$\mathbf{u}(\boldsymbol{r}) = \int \mathbf{J}(\mathbf{r}, \mathbf{r}')\mathbf{f}(\mathbf{r}')d^3r'. \quad (2)$$

The Oseen tensor can also take into account the presence of a wall (e.g. the oocyte cortex) where the velocity vanishes. These equations of motion for a microtubule are supplemented with the boundary conditions that the minus-end is fixed in space, while the plus-end is free to move.

Before advancing to a detailed mathematical analysis, we approximated microtubule motion under simplified physical conditions. Because the $\boldsymbol{F}_k$ kinesin forces are acting, on average, tangent to the microtubule all along its length, they will cause buckling if the microtubule is long enough. To understand this, we can make use of buckling theory for a rod supporting a load. Consider a section of microtubule of length L. The critical buckling force the load must apply is $f_B = \pi^2 C/L^2$ if the directions of the end segments are not constrained. This will differ by a factor of

order unity if there are such end-constraints, or if the load is distributed evenly over the rod rather than being confined to its ends. The longitudinal force f_L, due to kinesin, as discussed above, is $f_L = f_k L$. As L increases, f_L will increase and f_B will decrease. The point at which they are equal, gives the value of L at which buckling will first occur. The radius of curvature (R) for buckling will be proportional to L and will occur at $R = \left(\frac{C}{\beta f_k}\right)^{\frac{1}{3}}$ where β is a constant that will be determined by a more rigorous analysis outlined below that will allow comparison of theoretical predictions to measured microtubule curvatures in oocytes. We emphasize that this simplified buckling analysis is not precise, because it assumes a static load. With each kinesin force tangent to its local microtubule axis, as a microtubule bends over time, it redirects those forces, implying that the load on the fiber is time-dependent. We now present a more complete analysis of this dynamic situation.

To understand the motion of a single microtubule, one must consider that the surrounding fluid creates drag on it. We first consider a single microtubule with a local drag coefficient ν, but with no long-range hydrodynamics. A full hydrodynamic treatment must include the motions of kinesins on many adjacent microtubules and the more complex flow field they generate. However for a simple single microtubule simulation, we will assume that the only effect of the other microtubules is to produce a constant fluid velocity field v_s, which we will regard as a fixed external parameter.

The single microtubule dynamics model is similar to one developed previously for filament bending in gliding assays on glass surfaces coated with motors (Bourdieu, Duke et al. 1995). However, our model is 3-dimensional in an external fluid velocity field, rather than 2-dimensional with no external velocity field. The configuration of the microtubule, $\mathbf{r}(s)$, is parameterized as a function of arclength, s. Assuming drag is only local and writing out the forces on the right hand side of Eq. 1 explicitly,

$$\nu \frac{\partial \mathbf{r}}{\partial t} = -C \frac{\partial^4 \mathbf{r}}{\partial s^4} + \frac{\partial}{\partial s}\left(T(s) \frac{\partial \mathbf{r}}{\partial s}\right) - f_k \frac{\partial \mathbf{r}}{\partial s} + \nu \mathrm{v}_s \hat{k} \qquad (3)$$

where the position dependent tension $T(s)$ enforces the inextensibility of the chain $|\frac{\partial \mathbf{r}}{\partial s}|=1$.

We can now use Eq. 3 to determine the 3-dimensional motion of a microtubule subjected to kinesin forces while its minus-end is tethered in free space. Mathematical analysis yields a set of traveling wave solutions for long chains. The equation for their shape can be mapped onto the equation for a spherical pendulum and their form can be analyzed in several situations. For the case $\mathrm{v}_s = 0$ there are circularly rotating solutions with angular velocity $\omega = f_k/(\nu R)$, where R is the radius of curvature. We have studied numerically how R depends on the fluid velocity field and found it is quite insensitive over a wide range of v_s velocities. The precise value of R is determined by the boundary conditions, so we applied boundary

conditions numerically that held the minus-end at a fixed location but allowed it to pivot, while the plus end was completely free. Starting from random initial conditions, the equation rapidly goes to a steady state that typically is described by a curve that asymptotically becomes a helix that rotates uniformly at constant angular velocity ω (Figure 2.7, Movie S5). The crumpled initial conditions are clearly not attainable with a real microtubule, but are shown to demonstrate that, even from such extreme starting configurations, the dynamics approach the same helical solution. The handedness that develops for the helix is random, but is stable once steady state is attained. A combination of this numerical work and our analytical results agree with our much simpler buckling analysis discussed above that gives $R = \left(\frac{C}{\beta f_k}\right)^{\frac{1}{3}}$ and also agree with the power law found previously (Bourdieu, Duke et al. 1995). But now we can determine that $\beta = 0.05 \pm 0.0005$. The asymptotic radius varies only slightly over a wide v_s flow field velocity range.

We have studied variants of this model in which the boundary condition of the tethered minus-end is altered such that it is no longer freely hinged about a fixed point, but rigidly oriented in one direction. This, plus the stiffness of the microtubule, shifts bending for the first circular wave away from the minus-end. We have also studied the influence of a short ranged repulsive wall potential that is positioned near the minus-end and parallel with the flow field. This acts as a barrier similar to the oocyte cortex. The solution allows traveling waves, but for most values of the imposed fluid flow velocity (v_s) the waves evolve into cycloidal or sinusoidal

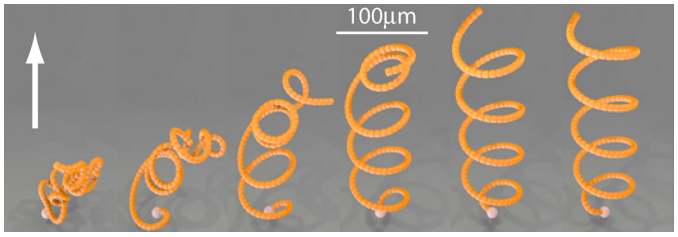

Figure 2.7 Single filament bending behavior generated by kinesin forces and an externally imposed fluid flow. Six time-points from a 200 frame simulation of a microtubule-like filament with its minus-end fixed in space (white ball) but free to rotate (see Movie S5 and Supplemental Information, Section 4.6). Starting from initial random compressed configurations of the filament (left side), tangent forces from kinesins walking toward the free plus-end, combined with an externally imposed fluid flow field (arrow) generates a stable rotating helical wave. Reasonable values for microtubule stiffness, kinesin force, and fluid viscosity produce a final radius of curvature between 25 and 61µm. For viewing purposes, the diameter of the filament here is 2000-fold that of a microtubule.

configurations parallel to the barrier, because the helix solution would violate the constraint of the wall. This behavior can also be understood in detail analytically, in excellent agreement with the simulations.

To determine if the wave-like behaviors in the simplified model simulations have similarities to real microtubule bending behavior in oocytes, we examined analytical solutions using elastic constants for microtubules of C=0.5 to $2\times10^{-23}\ Nm^2$, as reported previously (Felgner, Frank et al. 1996); (Gittes, Mickey et al. 1993). With a kinesin velocity of 780nm/s, cargo diameter/spacing a/d between 0.28 and 1, and assuming a cytoplasmic viscosity in fast streaming oocytes of 8 times that of water (Luby-Phelps 2000), the radius of curvature R is predicted to be 25-61μm and the wave period τ is predicted to be 203-405s. We performed gliding assays in order to compare *in vitro* radius of curvature numbers to what we could attain mathematically. While gliding assays are primarily used to perform motility assays on microtubule motors, here we were interested in microtubules that encounter a non-functional Kinesin-1 protein. When this occurs, the leading end of the microtubule sticks for a period of time to this kinesin, but the other functional kinesins continue to apply force to the microtubule. This causes the microtubule to bend and spiral around this non-functional kinesin, until the microtubule becomes unstuck and continues on its way. We measured the curvature of these microtubules in several gliding assays in order to provide biologically relevant numbers in our physical mathematical models. Figure 2.8 shows an example frame from one of the movies (Movie S9) taken on a wide field

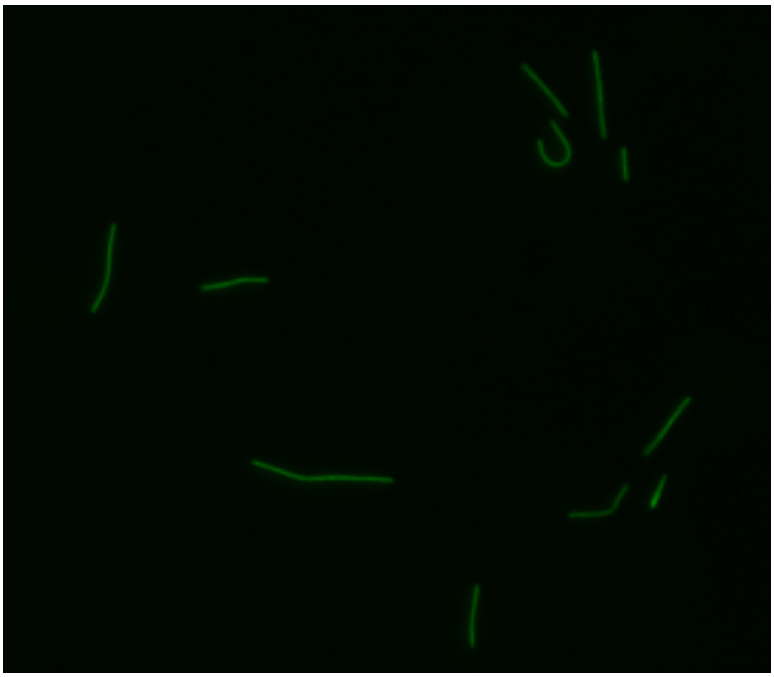

Figure 2.8. GFP-tubulin microtubules in gliding assay.
One frame from a microtubule gliding assay. Microtubules were polymerized from tubulin monomers from Cytoskeleton, and slide was coated with Kinesin-1 proteins. The curved microtubule in the top right of the image is spiraling around the leading end of the microtubule, which has encountered a non-functional Kinesin protein. Curvature was measured from this and other spiralling microtubules.

microscope of an active gliding assay. In it there are several spiraling microtubules. Curvature was measured in ImageJ using a three-point circle calculator. Average radius of curvature of an *in vitro* microtubule is 14.59 μm, s.e.m.=1.4, n=36.

For *in vivo* comparison, time-lapse confocal fluorescence microscopy was used to image GFP-tubulin microtubule arrays during fast streaming in stage 10B-11 oocytes. The average minimum array curvature radius was R = 19.5 $\pm$ 5μm (n=9). For arrays that remained in the optical section for sufficient time to determine wave velocity, τ was measured to be 294s (n=4) (see Experimental Procedures). These values are close to those predicted by the single microtubule bending model, suggesting that its physical explanation for oocyte microtubule bending is fundamentally correct.

Self organization of many microtubules using simulation

To develop a more realistic model, the same physical ingredients were considered, but with an array of 100 filaments tethered by their minus-ends to a cortex-like barrier plane at which both fluid and filament velocities must be zero. Furthermore, fluid flows were not externally imposed, rather they were generated internally by kinesin motion toward plus-ends. Thus, kinesin force and microtubule motion coupled to the surrounding fluid should generate a complete hydrodynamic model as described by Eqs. 1 and 2. Constant kinesin velocity toward plus-ends is combined with Eq. 2 to evolve the system in time. The added complexity of this

system pushes solutions beyond the scope of current analytic treatments, but it can be modeled numerically. We focused on three general questions: 1) Can a collection of many microtubules acted on by kinesin forces spontaneously self-organize into aligned arrays and undergo correlated bending, as observed in fast streaming? 2) Can parameter changes within this model explain the transition from slow to fast streaming? and (3) If so, what parameters control that transition?

The microtubule-like filaments were modeled with their minus-end pivot points tethered at height H above the cortex-like barrier, representing a height at which microtubules that are constrained by minus-end segments rigidly oriented within the cortex could bend enough to lie parallel to it. The semiflexible nature of the filaments and their interactions with each other were ensured by modeling them as chains of balls with spring potentials between them and next nearest neighbor repulsive potentials. The equilibrium distance between adjacent balls in a chain was 1 in the units used for the simulation. In Figure 2.9A and B, adjacent minus-end tether points are separated by 2 units, and chain lengths were 16 units. In simulations, two distinct behaviors of the system emerged. First, at very high kinesin generated force density or with filaments close to the barrier (*e.g.* $H = 1.0$), bending dynamics did not become well ordered (Figure 2.9A, and Movie S6). In addition, at very low kinesin generated forces ordering did not occur except at very long times. Small groups of filaments did correlate over short distances for brief time periods, creating patterns similar to those observed for microtubules in slow streaming oocytes (Figure 2.9C,

Movies S1 and S6), but long-range correlations did not develop. In the second behavior, simply shifting minus-end pivot points to a greater height above the barrier ($H = 2.0$) allowed a striking self-organization of filaments into uniformly oriented bending arrays that lay parallel to the barrier (Figure 2.9B, Movie S7). Some filaments at the array edges, where there were few neighbors, exhibited independent helical behaviors akin to those of the single filament simulation (Figure 2.7, Movie S5), but those with a full set of neighbors exhibited strongly correlated bending dynamics similar to those of microtubules in fast streaming oocytes (Figure 2.9D, Movies S2, S3, S7). Repeated trials identified parameters that favor this correlated behavior: intermediate filament stiffness akin to that measured for microtubules (Felgner, Frank et al. 1996); (Gittes, Mickey et al. 1993), intermediate kinesin force densities along the filaments, and minus-end pivot points above the wall at a distance equivalent to the spacing between microtubule minus-ends. With a spacing between microtubule tether points of 2 units and with the intermediate values for stiffness and force held constant, the transition between weak and strong correlation occurred near a height $H = 1.5$ units for chain lengths of 16 and 32, and for filament populations of 50 to 100. This suggests that the shift of the distance away from the cortex at which microtubules can form a parallel layer is an important parameter for controlling the transition from slow disordered to fast ordered streaming.

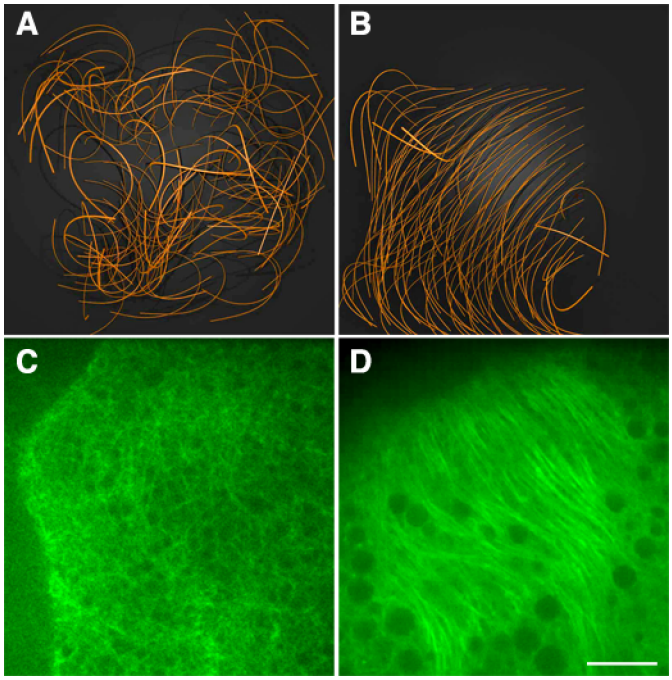

Figure 2.9 Correlated microtubule array bending generated by kinesin shear force between fluid and filaments near a membrane barrier. A, B) Views from above arrays of 100 microtubule-like filaments with minus-end pivot points at two elevations (A) $H = 1.0$ and (B) $H = 2.0$ above a cortex-like wall that suppresses filament and fluid motions near it. These are outcomes after 200 iterations of simulations under the following conditions: 1) spacing between minus-end pivot points of 2 units; 2) initial randomized filament configurations; 3) kinesin-like fluid-filament shear forces tangent to each filament axis at all points; and 4) fluid movements generated exclusively by the kinesin-filament shear forces (see Movies S6 and S7). Note the largely non-correlated bending behavior in A versus the correlated bending behavior in B. Shown in C and D) are confocal images of GFP-α-tubulin at 0-10um distance from the oocyte membrane. C) Stage 10A slow streaming (see Movie S1). D) Stage 10B fast streaming (see Movies S2, S3). Scale bar = 10μm for C and D.

To test the model, we considered ways to alter key parameters in living oocytes and compare their effects on streaming with those predicted by the model. There is currently no way to alter H, but kinesin mutations provide a means to alter force density on microtubules. *Khc*^{23} *and Khc*^{17} are two well characterized mutant alleles of the *kinesin heavy chain* gene that, by changing single amino acids in the force-generating head domain, cause 3.8-fold and 1.6-fold slowing, respectively, of motor velocity on microtubules (Brendza, Rose et al. 1999). Slowed kinesin velocity, when used in model simulations with $H = 2.0$, are predicted to reduce the force density along microtubules, which would reduce bending force and slow the rate of fluid flow toward plus-ends. The predicted outcome is that the evolution of filament alignment will be delayed substantially and the velocity of the eventually attained correlated cytoplasmic streaming is reduced. In stage 10B-11 wild-type oocytes, correlated streaming velocity was 217+/-38nm/sec (n=12 oocytes). In stage 10B-11 mutant oocytes, three different types of streaming behavior were observed: 1) uniform non-correlated patterns of yolk particle motion (*Khc*^{23}, 26 $\pm$ 5 nm/sec, n= 12 and *Khc*^{17}, 38 $\pm$ 6 nm/sec, n=12); 2) non-uniform patterns with small patches of correlated streaming; and 3) uniform correlated streaming at slowed velocity (*Khc*^{23}, 79$\pm$19 nm/sec, n=12 and *Khc*^{17}, 102$\pm$31 nm/sec, n=12). The three states in the mutants could reflect different stages in a slowed self-organization, consistent with the prediction from the model. Alternatively, they could reflect three different stable states. Because oocyte physiology is robust for only ~1hr post dissection, long-term time-lapse imaging that could address this question was not fruitful. Advances in

observation techniques and tests of additional model parameters, for example attractive forces between microtubules from crosslinking factors and modeling an oocyte-like concave rather than a planar barrier, could provide additional important insights into the streaming mechanism.

Discussion

In general, processes involving the transport of protein complexes, cytoskeletal polymers and organelles with a strong directional bias should be profoundly affected by hydrodynamics, because at low Reynolds number the motions of distant objects are coupled through viscous drag. Elegant studies of pronuclear migration in sand dollar zygotes established that there can be length-dependent pulling forces on astral microtubules emanating from a centrosome (Hamaguchi and Hiramoto 1986). The authors suggested that such forces are generated by drag on organelles that are carried toward minus-ends that are attached to the sperm pronucleus centrosome. It has since been shown that drag on minus-end directed dynein motor complexes indeed generates important length-dependent pulling forces on microtubules attached to pronuclei (Kimura and Kimura 2011); (Longoria and Shubeita 2013); (Shinar, Manab et al. 2011). Our work presented here has focused on what is in essence the reverse process: predominantly plus-end directed transport driven by kinesin-1 along microtubules that are tethered by their minus-ends to a cortex. In contrast to the microtubule straightening-pulling effects of dynein walking toward anchored minus-ends, kinesin movement away from anchored minus-ends

causes cortical microtubules to buckle and, under some conditions, to self organize into bending parallel arrays. Drag on the kinesin-cargo complexes that move on those bending microtubule arrays drives long-range fluid flows in constantly varying directions.

In developing oocytes, the timing of the switch from mid-stage slow streaming to late-stage fast streaming is crucial. If fast streaming occurs too early, the proper concentration and anchorage of key body axis determinants at their cortical sites fails and subsequent embryo development proceeds without normal patterning (Theurkauf 1994); (Manseau, Calley et al. 1996). On the other hand, if streaming-mediated mixing does not occur, embryos fail to develop beyond the early cleavage stages (Serbus, Cha et al. 2005). Our hydrodynamic modeling shows that oocytes could control the slow-fast streaming transition by changing a single parameter H: the distance between the cortical barrier plane and the underlying layer at which cortically tethered microtubules can align. This is because fluid motion between the barrier plane and the microtubule layer makes an important contribution to hydrodynamic coupling and thus to the correlated behavior of neighboring microtubules. Since for fast streaming, the critical distance of microtubules from the barrier is approximately twice the distance between microtubule tether points, the inward shift away from the cortex need not be large. High resolution fluorescence images of stage 9 oocytes (Parton, Hamilton et al. 2011) suggest a spacing of cortical microtubules from one another of roughly 1mm. Thus, a spacing between the cortical

barrier and the microtubule layer of ~1*m*m could be sufficient to allow the transition from slow to fast streaming. Evidence consistent with a multi-micron inward shift of microtubules during the slow to fast streaming transition has been reported (Wang and Riechmann 2008). How such a shift could be accomplished while keeping minus-ends tethered is an interesting question. One possibility is that if the initial segments of microtubules are rigidly oriented and if they emerge from the cortical plane at an average angle of 90 degrees, their stiffness would define the radius over which they could bend to form a subcortical layer and thus the distance between the two planes. Future ultrastructural analysis of the organization of microtubules and the cortex during fast streaming could provide important new insights into how the slow-disordered to fast ordered streaming transition is controlled.

Other model parameters influence the slow-fast streaming transition: the microtubule stiffness, kinesin velocity, microtubule spacing, and cytoplasmic viscosity. Because a reduction in viscosity induces long range ordering, this alone should account for the transition seen from slow to fast streaming. Further evidence for this is the premature fast streaming that is induced by lowering the viscosity of the cytoplasm through f-actin depolymerization (Theurkauf 1994); (Dahlgaard, Raposo et al. 2007). If instead, one reduces the force density on microtubules by lowering kinesin velocity, this decreases bending, fluid velocity, and hydrodynamic coupling of neighboring microtubules, which greatly slows correlated alignment. Our tests of slow-*Khc* mutant oocytes confirmed that reducing kinesin velocity indeed inhibits correlated

alignment and streaming velocity. Model simulations also show that high force density on cortical microtubules will increase microtubule bending to the point that the self-organizing correlated state cannot evolve. Consistent with this, stabilizing the f-actin meshwork in ooplasm, which should sustain high viscosity and thus high kinesin generated force density on microtubules, prevents the transition to fast streaming in stage 11 oocytes (Dahlgaard, Raposo et al. 2007). Conversely, destabilizing f-actin allows premature fast streaming in stage 8-9 oocytes (Theurkauf, Smiley et al. 1992); (Dahlgaard, Raposo et al. 2007); (Manseau, Calley et al. 1996). Thus, intermediate conditions for force transfer between kinesin, microtubules, and cytoplasmic fluid, along with sufficient distance between the microtubule layer and the cortical barrier are ideal for rapid self organization into the fast streaming state.

Interestingly, model simulations show that increasing the separation distance between the subcortical microtubule layer and the cortical wall (beyond 2 units) facilitates more rapid alignment into parallel arrays, but the amplitude of bending becomes much smaller. Considering the purpose of fast streaming in oocytes, this suggests that the transition from slow to fast streaming re-sets the self-organization parameters such that the system is at the edge of a symmetry-breaking phase where there is sufficient order to align microtubules and generate robust fast cytoplasmic flow, yet enough bending of the arrays to facilitate semi-chaotic variations in flow directions. In regard to a need for such variation, rigorous analysis in two dimensions using the Thurston-Nielsen classification theorem has shown that topological chaos is

crucial for efficient fluid mixing (Thurston 1988). This is particularly the case for the low Reynolds number regime of small scale and high viscosity in an oocyte. Thus, control of the stage 10A to 10B parameter transitions for encouraging both fast flows and bending pattern variation is likely a crucial element for successful mixing of oocyte and nurse cell cytoplasm.

Chapter 3

Impellers and Other Studies

Introduction

Our work in the last chapter focused on the physical properties behind the mechanism of streaming, and the roles microtubules and Kinesin-1 play in streaming. Another avenue to explore is whether any cargoes carried by Kinesin act as an impeller during streaming.

One possible streaming impeller is the lipid droplet. This is supported by the observation that in streaming oocytes, lipid droplets are found in close proximity to microtubules, whereas other organelles are excluded from this region (Theurkauf, Smiley et al. 1992) (Image 3.1). In order to study the role of lipid droplets in streaming, I looked at the lipid droplet associated protein Klarsicht. Klarsicht, or Klar, is a regulating protein of microtubule motors in Drosophila that was first characterized in the early developing Drosophila embryo (Welte, Gross et al. 1998), when neutral lipid storage vesicles, called lipid droplets, are transported to the periphery of the embryo. Klar mutants show disturbed transport of these lipid droplets, causing the embryos to appear more or less transparent (Wieschaus and Nüsslein-Volhard 1986). Klar is a crucial player in regulating the bidirectional transport of lipid droplets; in Klar mutants, bidirectional transport of lipid droplets was impeded. However, the only organelle affected was lipid droplets, implying specific targeting of Klar (Welte, Gross et al. 1998). The protein is found in

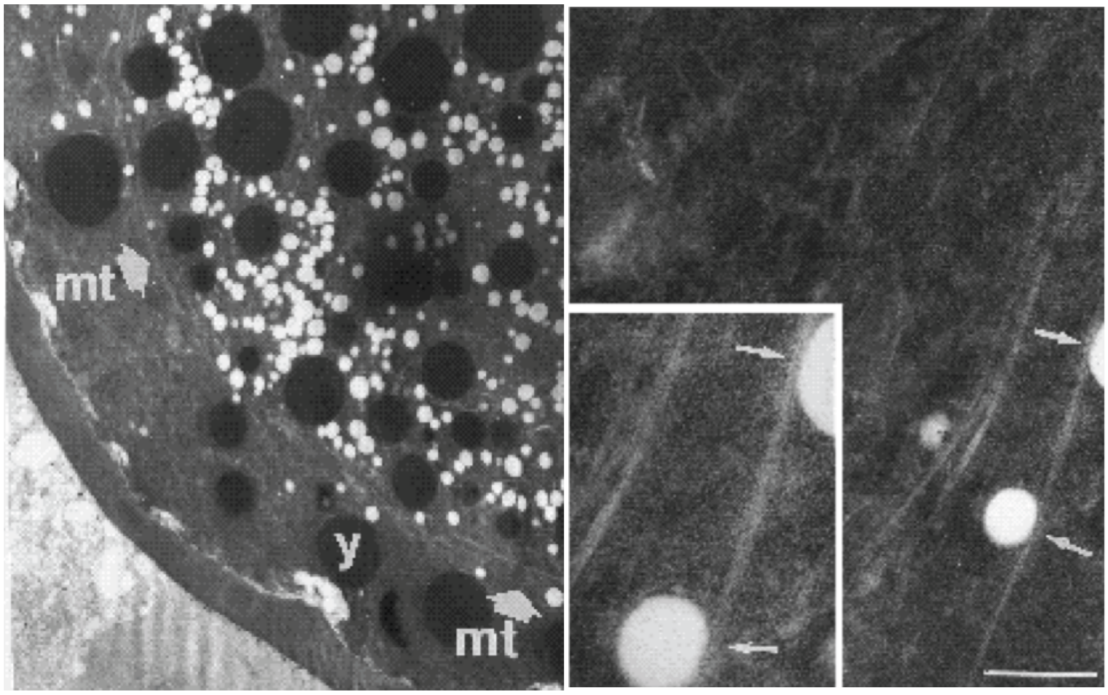

Figure 3.1. Electron micrograph of stage 10b oocyte. On the left is a micrograph of an oocyte approximately 4 μm wide. Subcortical microtubules are indicated by the arrows, and yolk endosomes are seen here as black circles. The white circles are lipid droplets, and are excluded from the area between the cortex and the subcortical microtubules. The yolk endosomes are seen on both sides of the microtubules. On the right is a higher magnification view of lipid droplets closely associated with microtubules. The white bar in the right corner is 300 nm. (Image from (Theurkauf, Smiley et al. 1992).)

conjunction with dynein in immunofluorescence assays, and has been shown to form a complex with Kinesin-1 (Welte, Gross et al. 1998); (Shubeita, Tran et al. 2008); (Gaspar, Yu et al. 2014), suggesting that it may coordinate which motor is active on a cargo at a given time (Gross, Guo et al. 2003); (Gross 2003); (Welte 2004). Klar mutants also show disturbed nuclear migration in the imaginal disc of the eye (Welte, Gross et al. 1998); (Fischer-Vize and Mosley 1994).

The Klar gene spans approximately 110 kb of the fly genome, and contains 19 exons (Kim, Cotton et al. 2013). There are five confirmed protein isoforms, two of which contain a lipid droplet binding domain (β and ε), and 3 of which include a nuclear envelope-targeting domain known as the KASH domain (α, γ, and *δ*) (Mosley-Bishop, Li et al. 1999); (Starr and Han 2002); (Guo, Jangi et al. 2005); (Yu, Li et al. 2011). The sequence for the KASH domain is located in exon 18. The lipid droplet binding isoforms are alternatively spliced to include a 640 base pair extension to exon 15 (Guo, Jangi et al. 2005); (Berkeley Drosophila genome project), which when included with exon 15 is referred to as 15x, which contains an in-frame stop codon. Thus, exons 16-18 are not included in the β and ε messages of Klar, and thus this isoform lacks the nuclear-envelope-targeting KASH domain. The α and β mRNAs are transcribed from a promoter in exon 0, whereas the *δ* and ε promoter is located in exon D, between exons 4 and 5. The promotor for the γ isoform is between exon 15x and exon 16; its function is currently unknown (Kim, Cotton et al. 2013) (Figure 3.2).

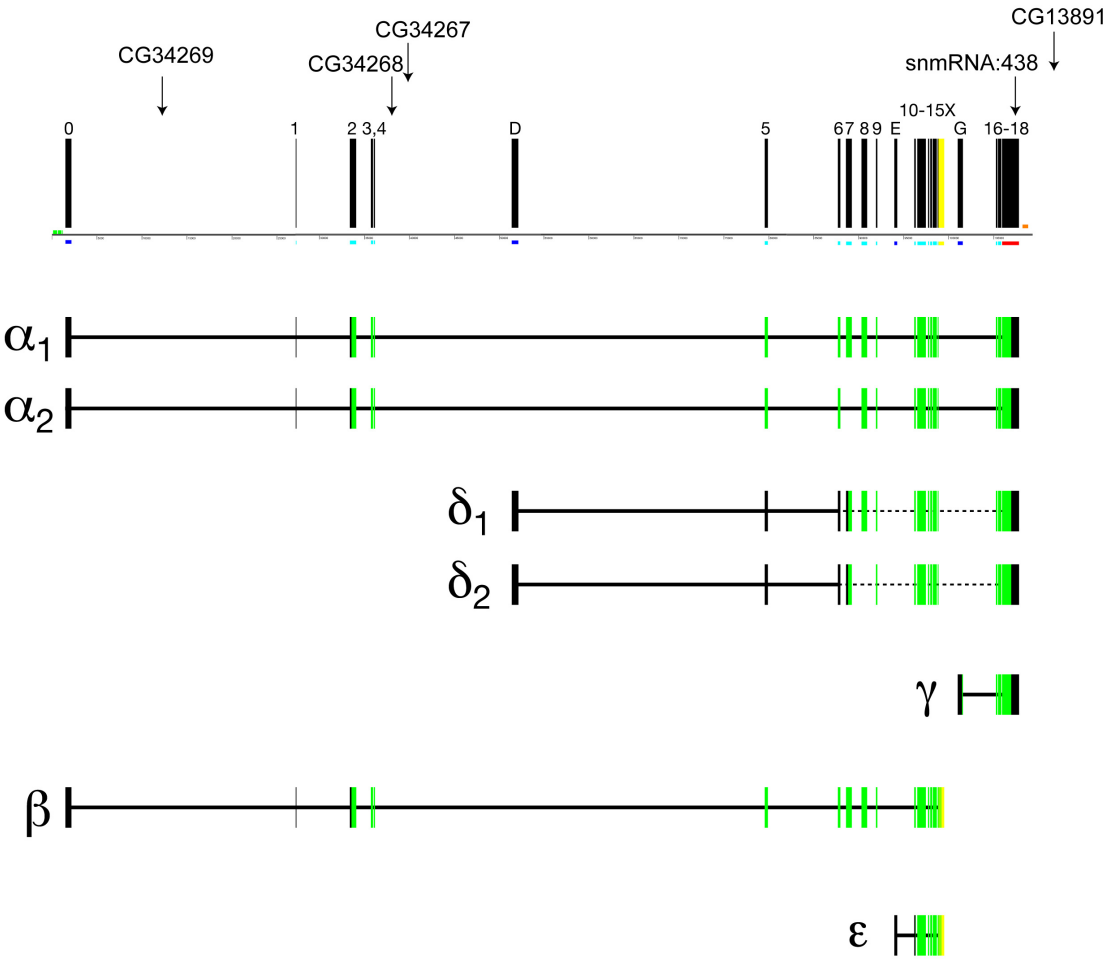

Figure 3.2 Overview of *Klar* locus. At the top of the image is the *klar* gene in the left arm of the third chromosome. Exons are represented by black vertical bars and are labeled with their number or letter above the bars. Other small putative genes are shown where they may occur in introns and are labeled with CG and a number. Different isoforms are shown with which exons they include. Beta and epsilon are the lipid droplet binding isoforms. (Image from Michael Welte.)

Several mutations affect the lipid droplet binding protein isoforms. These include mutations that excise a number of exons, that introduce a stop codon in exon 15, or are in the promoter and prevent Klar from being expressed. In order to study whether the lipid droplet isoforms of Klar are involved in the process of cytoplasmic streaming, I looked at mutants Δ515, Klar1, YG3, and KlarMW. Δ515 is a deletion mutant that removes exons 5-15, and is effectively a null mutation, but leaves intact certain small predicted genes in earlier introns without which the mutant flies are not viable (Michael Welte, personal communication). The Δ515 mutant removes most of the Klar message of all isoforms. As this mutation is generally lethal when homozygous, the heterozygous mutant must be crossed with a deficiency strain, Df(3L)emcE12, which deletes the klar locus along with several surrounding genes. Klar1 introduces a stop codon in exon15, which truncates the protein before the lipid binding domain can be included. YG3 is a mutation in the promotor region of α and β isoforms. KlarMW specifically deletes a 25 bp region of exon 15x, which codes for the lipid droplet binding domain. The mutation causes a frameshift and a trunctation of much of the lipid binding domain (Yu, Li et al. 2011) (Figure 3.3).

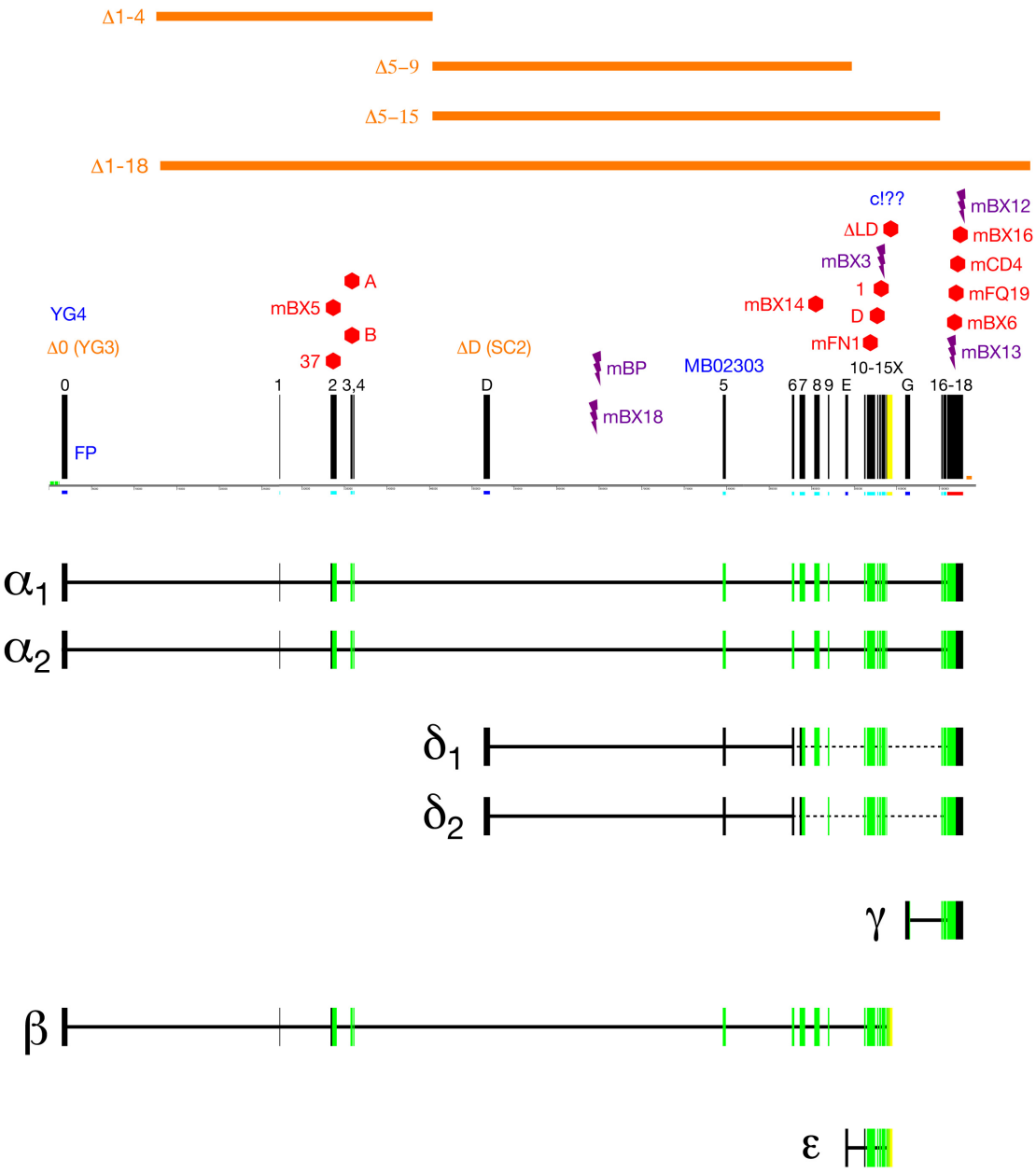

Figure 3.3. *Klar* mutant alleles. As in the previous figure, exons are represented by vertical black bars over the *klar* locus, and different isoforms are shown below. Different mutations are represented here above the locus. In orange are deletion mutations, such as Δ515 and YG3. Red stop signs show nonsense mutations, purple lightning bolts show chromosomal breaks, and mutants in blue are poorly understood. (Image from Michael Welte.)

Results

To gain insight into whether lipid droplets are involved in the mechanism of cytoplasmic streaming, I used confocal microscopy to image live oocytes dissected from female *Klar* mutant flies of several different strains. First, I replicated an experiment done in Klar 1 mutant flies, as slowed cytoplasmic streaming had been observed in this line (Michael Welte, personal communication). This mutation introduces a stop codon in exon 15, before the exon containing the lipid droplet binding domain. I injected flies with Trypan blue approximately two hours before dissecting oocytes in halocarbon oil. Trypan blue fluoresces red when observed with a 590 nm wavelength laser, and is taken up in the yolk endosomes of the oocyte from the female abdomen. The yolk endosomes are then visible and can be used to determine the velocity of cytoplasmic streaming. I used female 700W flies as a control. Comparison of streaming velocity in the control to Klar 1 mutants is striking: while streaming still takes place in the mutants, it is at approximately 25% wildtype velocity. Average control velocity in this experiment was unusually fast at 463 nm/s, and average Klar1 velocity was 136 nm/s (for standard error and p-values for all mutations observed, refer to Table 3.1 and Figure 3.4). I then observed streaming in Δ515 mutant flies, which arose from a different mutagenesis experiment than Klar 1. The velocity of streaming in Δ515 flies is even slower than that of Klar1 flies, at just 70 nm/s. When the two lines were crossed with each other to rule out background

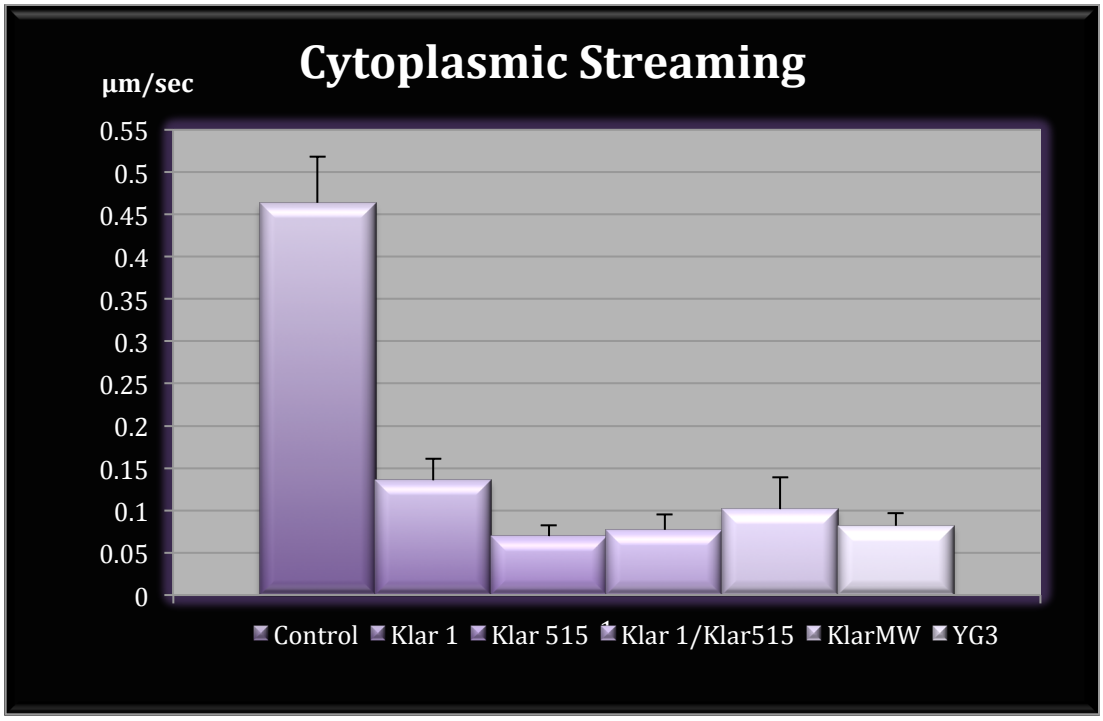

Figure 3.4. Results from tracking velocity of cytoplasmic streaming in *Klar* mutants. All *Klar* mutants studied show significantly reduced streaming, particularly the deletion mutant Δ515. Velocity is showed on the y-axis and genotype is displayed on the x-axis. N=5 for all genotypes quantified.

Genotype	Average Velocity	Standard Error	p-value
Control	0.463 µm/s	0.055	
Klar 1	0.136 µm/s	0.026	0.0020
Klar 515	0.070 µm/s	0.013	0.0015
Klar 1/515	0.077 µm/s	0.018	0.0013
Klar MW	0.102 µm/s	0.038	0.0009
YG3	0.082 µm/s	0.015	0.0016
KlarRNAiControl	0.093 µm/s	0.023	
Klar RNAi	0.077 µm/s	0.016	0.4647

Table 3.1 Velocity results from tracking cytoplasmic streaming in Klar mutants and RNAi. Genotype is listed in the left-most column, followed by the average velocity, standard error of the mean, and p-value compared to the control used. P-values for all mutants show significance, while results from the *klar* RNAi do not. N=5 for all genotypes measured.

genetic effects, velocity remained low at 77 nm/s.

In order to determine whether the ε isoform is involved in driving cytoplasmic streaming, I observed streaming in the YG3 Klar mutation, which contains a small mutation in the promotor for the α and β isoforms. This abolishes expression of the β isoform, which is the main lipid droplet binding isoform; however, it leaves the ε isoform intact. In this mutant, streaming velocity was measured at 82 nm/s, a similar velocity to what is seen in the Δ515 mutant. Since the Δ515 mutant affects the expression of all isoforms, but the YG3 mutation only affects the α and β isoforms, these data imply that the ε isoform is not involved in driving cytoplasmic streaming.

The last mutant in which I observed streaming was the KlarMW mutant, which contains a deletion in the middle of the lipid droplet binding domain. In KlarMW mutant oocytes, streaming velocity was 102 nm/s. The data from this experiment provide further support for the Klar1 mutant results.

While these data are very promising, I wanted to ascertain whether the effect could be from some unknown genetic background. I next looked at flies with RNAi against the *klar* message. The recognized sequence is in exon 6, which affects all isoforms aside from the γ isoform. In these oocytes, streaming velocity is slightly reduced, but not significantly (Figure 3.5). This result goes against the results found in the mutation studies. It is possible that the *klar* mutants contain background mutations that affect streaming; however, it is likely that *klar* RNAi is not strong enough to knock down sufficient mRNA to show an effect on streaming.

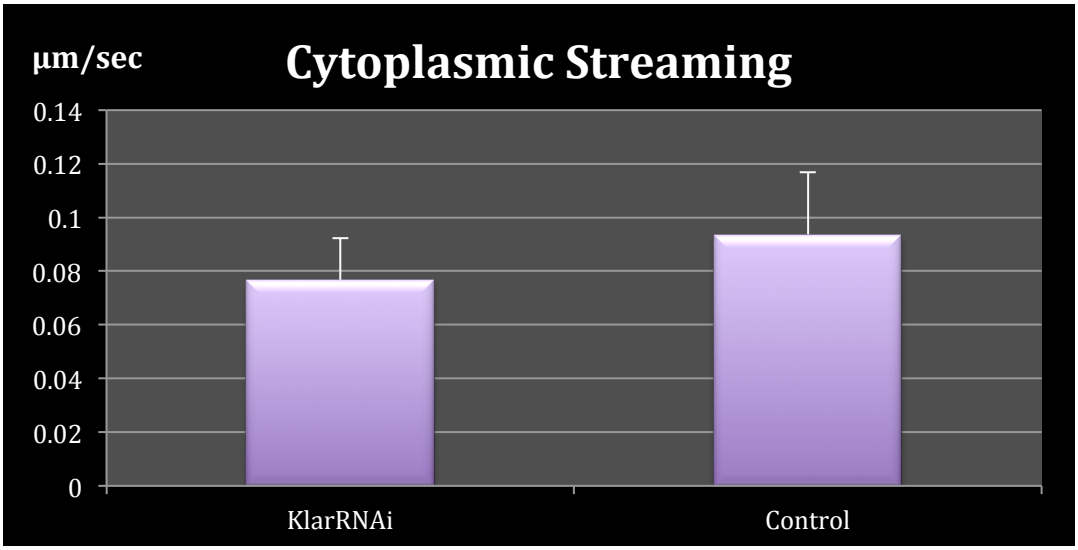

Figure 3.5 Results from tracking cytoplasmic streaming in flies treated with *Klar* RNAi. In *Klar* RNAi flies, streaming velocity was slightly reduced, but not significantly. Velocity is shown on the y-axis and genotype is shown on the x-axis. N=10 for both genotypes.

Discussion

My results with *Klar* mutants suggest that Klar and lipid droplets are involved in cytoplasmic streaming, and that the β isoform specifically affects streaming in oocytes. It is possible that lipid droplets serve as an impeller for streaming. Our results from mathematically modeling streaming showed that Kinesin-1 by itself can drive streaming if it is spaced closely on the microtubule. This might explain the reduction but not complete cessation of streaming; perhaps Kinesin is able to create some fluid flow, but lipid droplets complement the force put on the surrounding cytoplasm. Further mutant studies should include mutants that knock out the ε but not β isoform of Klar to ascertain whether the ε isoform has any effect on streaming, and mutants that knock out the α, γ, and *δ* isoforms, but leave the lipid droplet binding isoforms intact.

Another possibility is that lipid droplets are not acting as impellers, but Klar acts in its role as a motor regulator to inhibit dynein or otherwise affect the normal functioning of kinesin in streaming. While the lowered velocity of streaming in lipid droplet binding domain mutants would seem to imply that lipid droplets play a role, it is possible that somehow disrupting this region of Klar also affects its ability as a motor regulator in some fashion, or that lipid droplets carry Klar in from the nurse cells and so it is unable to reach the oocyte without this binding domain. This could be addressed both by using immunofluorescence to determine where Klar is in the streaming oocyte in these mutants and by looking at mutants which lack lipid droplets; the *midway* mutant does not produce lipid droplets in oocytes, but the

oocytes in these mutants generally stop developing before they ever get to the streaming stage. However, there is some evidence that disrupting the ecdysone pathway by crossing E75 mutants and *midway* mutants allows the oocytes to survive longer (Michael Welte, personal communication). It would be important to do an immunofluorescence assay to find where Klar localizes in these mutants as well.

The results from the RNAi of Klar are somewhat confounding. One possibility is that the genetic background of the *klar* mutants is causing the slowed velocity of streaming; this is unlikely to be the case as many of these mutants were developed in different ways, years apart from each other, and a cross between Klar 1 mutants and Δ515 mutants shows reduced streaming. Another possibility is that the RNAi against *klar* is not strong enough and is not knocking down a sufficient amount of message to adversely affect streaming. This could be addressed by using quantitative PCR to look at how much *klar* mRNA is present in streaming oocytes. Another way this could be tested is by observing clearing in developing *klar* RNAi and YG3 embryos. The YG3 mutant undergoes normal clearing in cycle 14, but does not cloud up again with lipid droplets; if the RNAi were knocking down sufficient amounts of Klar, I would expect this failure to cloud up after cycle 14 (Michael Welte, personal communication; (Welte, Gross et al. 1998).

Additional Studies of Cytoplasmic Streaming

In order to better hone the mathematical model of streaming, it is important to know such things as how the microtubules are organized at the cortex and how far apart they are from each other. Earlier electron microscopy has shown parallel microtubules just below the cortex (Figure 3.1) (Theurkauf, Smiley et al. 1992), but these studies were not detailed enough to determine microtubule spacing or organization at the cortex.

In order to keep the internal structure and organization of the oocytes as close to life-like as possible, I attempted to use a high-pressure freezing technique in order to prepare the oocytes for electron microscopy. This method freezes samples in a matter of milleseconds, as opposed to chemical fixation, which takes longer to perfuse the sample, particularly with large samples such as whole cells (McDonald 1999). In this method, samples are placed in a small metal carrier with an indentation in the center for the sample, and then this carrier is capped and put into a high pressure freezer. The sample must not contain any air bubbles, so in the case of oocytes, the area surrounding the oocytes must be filled with a viscous fluid that will allow rapid freezing to occur. I used two different fluids: 20μm/μL bovine serum albumin (BSA), and 20% glycerol. The small volumes of BSA dried out too quickly for the samples to be used, but I was able to image samples placed in 20% glycerol (Figure 3.6 and Figure 3.7).

Despite seeing a few microtubules in these micrographs, there were not as many as expected, and when I used confocal microscopy to determine whether oocytes

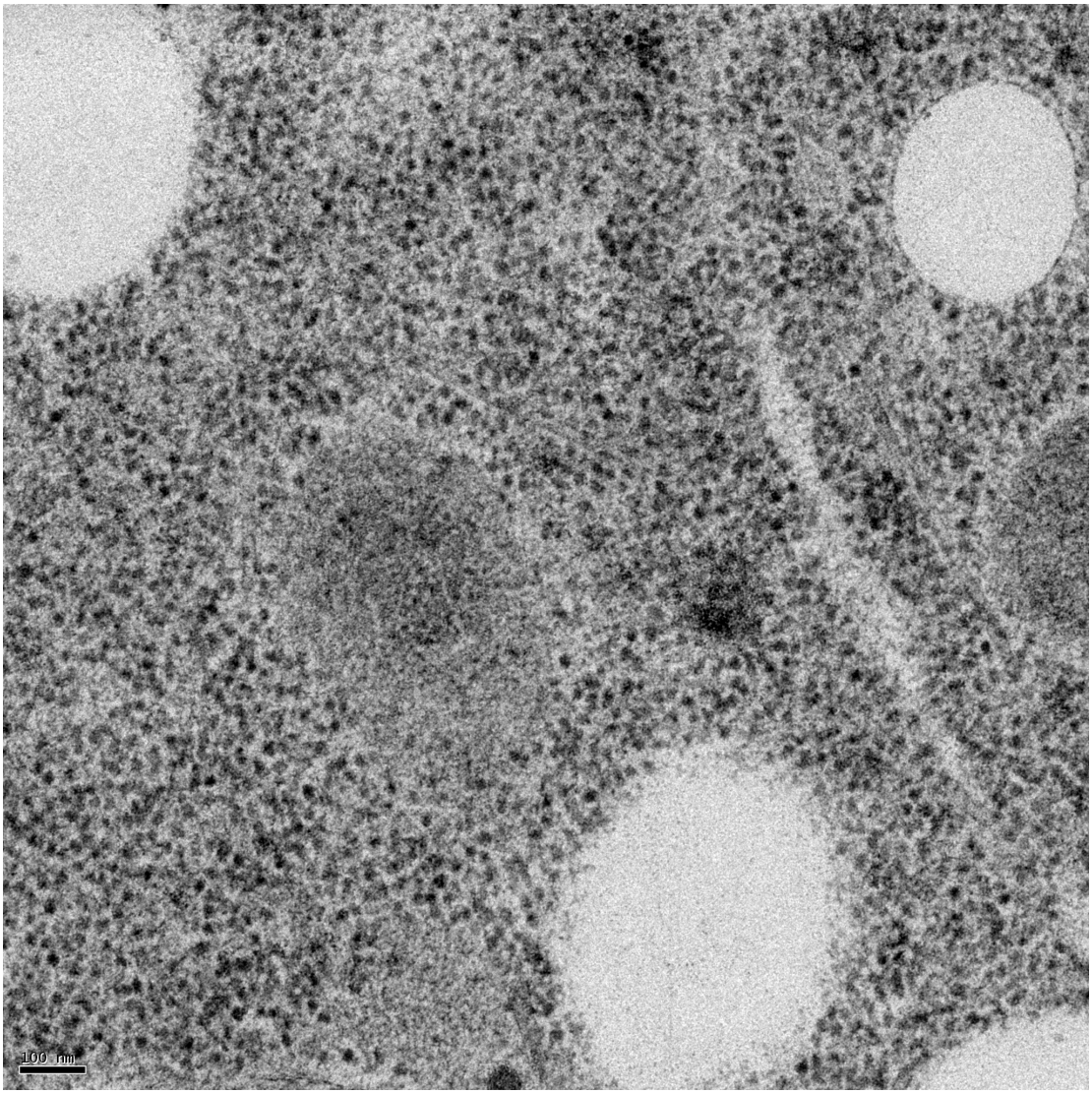

Figure 3.6 Electron micrograph of *Drosophila* oocyte with few microtubules. In this micrograph, a few microtubules are evident at the center of the image. This area contained the most microtubules of any area we imaged. Scale bar is 100 nm.

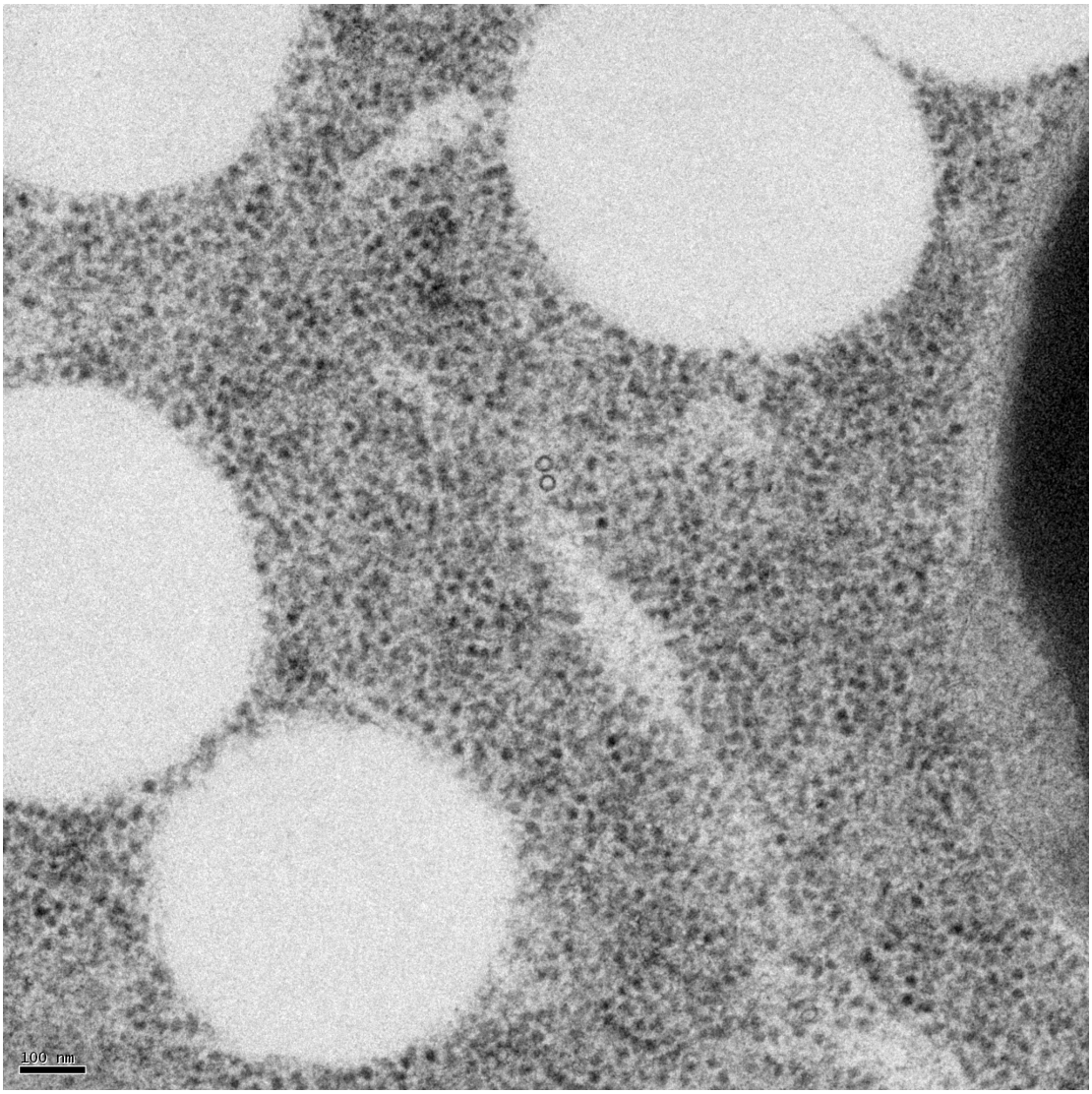

Figure 3.7 Electron micrograph of *Drosophila* oocyte with cross-sectioned microtubules. In this micrograph, there are five lipid droplets and the edge of a yolk endosome. Of note are the two microtubules side by side in the center of the image. Scale bar is 100 nm.

were able to perform cytoplasmic streaming in 20% glycerol, I determined that they stopped streaming before I was able to image them. Further, the oocytes appeared shriveled and dead.

Next, I attempted to use chemical fixation in order to do standard electron microscopy. I used oocytes expressing GFP-tubulin and a fix of 1:1 cacodylic acid and 16% paraformaldehyde (after (Theurkauf, Smiley et al. 1992) and (Serbus, Cha et al. 2005)), and then used, variously, a primary antibody against GFP, a FITC-conjugated monoclonal antibody against tubulin, and a primary antibody against tubulin, in order to see whether parallel arrays of microtubules survived the fixation process. Results were inconclusive, as it is unclear whether the antibody has stained microtubules in the oocyte, microtubules in the follicle cells, or an artifact. (Figure 3.8).

Next, I developed some carriers with openings the same average width and height of an oocyte, to try again to do freeze fixation, but without the noncryoprotectant fluid around them. Instead, flies will be transferred with halocarbon oil. Halocarbon oil does not allow freezing to occur rapidly enough to preserve internal structure, but in small enough volumes with the oocyte able to touch the metal sides of the carrier, should not present a problem. I have not tested these yet, but this will be the next step in understanding more about the ultrastructure of the stage 10b streaming *Drosophila* oocyte.

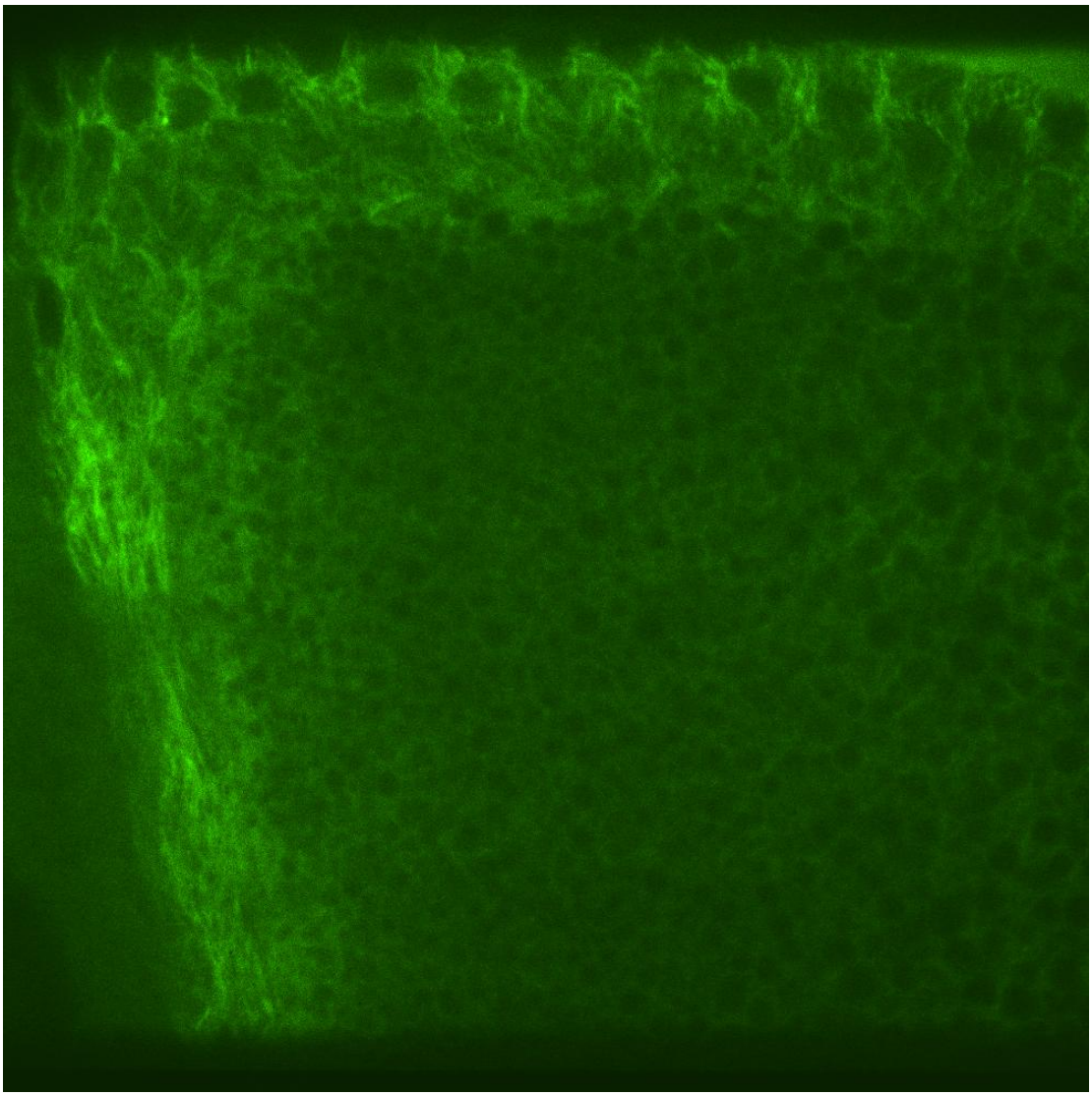

Figure 3.8 Fixed stage 10b oocyte stained with antibodies against tubulin. This oocyte was fixed with cacodylate and para-formaldehyde, treated with an antibody against tubulin, and then set in a fluorescence-conjugated secondary antibody. While there do appear to be microtubules, it is unclear whether they are part of the oocyte or only in follicle cells.

Chapter 4

Summary and Future Directions

The goal of my graduate research work was to further the understanding of the mechanism of cytoplasmic streaming. The work presented here demonstrates a number of novel findings with regard to this physical mechanism. It provides the first evidence that microtubules are not flowing with the cytoplasm, but are anchored by their minus ends at or near the cortex, through the use of FRAP and photoconvertible proteins. We show that with only an anchored field of microtubules, a force-producing motor, and the viscosity of cytoplasm, cytoplasmic streaming is possible. Our model can be improved by gaining more understanding of how microtubules are organized at the cortex, as well as how closely spaced they are. Future studies in electron microscopy may provide insight into these problems.

Previous research has suggested that there may be a cargo acting as an impeller pushing against the cytoplasm, but our findings show that it is possible for Kinesin-1 alone to act in this fashion, if it is sufficiently closely spaced on the microtubule. However, as previous work from our lab has shown that mutations in kinesin light chain cause a reduction in the velocity of streaming, it is likely that there is indeed an impeller.

The identity of this impeller remains unclear, but lipid droplets present a good candidate. My work with Klar shows preliminary results that mutations in this protein cause a significant, at least 4-fold reduction in the velocity of streaming. Further

studies should look at Klar mutants that affect non-lipid binding droplet isoforms of Klar, as well as mutants lacking lipid droplets. As the RNAi of this locus showed very little reduction in streaming, it will be important to discern how much reduction of mRNA there is in these oocytes. This can be done using quantitative PCR against this region using unfertilized embryos.

Chapter 5

Experimental Procedures

Genetics

To generate fluorescent microtubules in oocytes, *UASp-GFPS65c-α-tub84B* was expressed in the female germline using a VP16-GAL4 driver transgene (*P{w*$^{+}$ *GAL4::VP16nos.UTR}MVD1*). To obtain egg chambers that were homozygous for slow-*Khc* mutations, germline clones were induced using a FLP/FRT mitotic recombination approach in females heterozygous for either *Khc*^{23} or *Khc*^{17} as described previously (Serbus *et al.,* 2005). To obtain egg chambers in which photoconvertable protein Dendra2 is present on tubulin, female *w***; P{UASp-alphatub84B.Dendra2}5M* flies were crossed with male maternal triple driver Gal4 (*MTD-Gal4*): *(P(otu-Gal4*::*VP16.R)1*, *w[*]*; *P(Gal4-nos.NGT)40*; *P(Gal4*::*VP16-nos.UTR)CG6325[MVD1])* flies. To study Klar's role in streaming, various mutants were used. These lines included homozygous *[ru1] [klar1]* flies; Δ5-15 mutants over a balancer and crossed with deficiency strain *Df(3L)emc*^{E12}*,* as homozygotes are rare and quite weak; homozygous *KlarMW* flies; and homozygous Δ*YG3* flies.

Microscopy

Egg chambers were dissected from adult females and mounted live in halocarbon oil on coverslips then were imaged with an Ultraview (Improvision/BioRad) spinning disk confocal fluorescence microscope (Figure 1, Movies S1, S2) or an Olympus

FV1000 2-photon fluorescence microscope (Figure 2, Movies S3, S4). With the spinning disk scope, GFP-tubulin images were collected every 2 seconds. With the 2-photon scope, images were collected every 0.93 seconds. FRAP tests were performed using the Olympus FV1000 "bleach laser" function set to a wavelength of 880 nm for a duration of 0.24 seconds. Photoconversion tests were performed using a Mosaic Digital Illumination system on the Ultraview spinning disc confocal microscope using a broad-spectrum light. Yolk endosome streaming behavior was recorded using the spinning disk scope with oocytes from females whose abdomens were injected with Trypan blue two to four hours before ovary dissection. The dye is included with yolk during endocytosis. Endosome fluorescence images were collected every 2 seconds.

Immunofluorescence

Immunofluorescent studies were carried out by dissecting ovaries from GFP-tubulin-expressing flies and separating egg chambers. A 1:1 cacodylate:16% paraformaldehyde solution was injected under the oil drop and allowed to fix for 10 minutes. Samples were then rinsed in 0.1% Triton-PBS, and washed for 2 hours in 1% Triton-PBS. Next, samples were incubated overnight at $4^{\circ C}$ in a 0.01% Triton-PBS solution containing 1:100 DM alpha-tubulin FITC monoclonal antibody from Sigma Aldritch.

Quantification

Streaming velocities were determined for 12 oocytes per genotype by tracking net

position changes of 10 yolk endosomes over 50 seconds per oocyte. This low frequency sampling approach for each endosome essentially filters out the influence of short-range multi-directional saltatory motion, thus focusing velocity values on bulk cytoplasmic flow instead of random acto-myosin driven motions. Increasing sample sizes for endosomes per oocyte and for oocytes per genotype did not substantially change streaming velocities. Endosome tracking was performed in ImageJ version 1.42 using the MTrackJ version 1.5.0 plug-in (Meijering and Dzyubachyk 2012). Curve radii for microtubule arrays were measured from individual images of GFP-tubulin in fast streaming oocytes from time-lapse spinning disc confocal movies. For any clearly visible wave, the apex radius was determined by fitting with a circle. Wave velocities were measured by tracking position changes over time for curves that remained clearly defined for at least 4 consecutive frames. Photobleaching recovery was measured in ImageJ version 1.42 by determining at different time points the average pixel intensity of a 15μm long line along a 24μm path that was perpendicular to the long axis of the bleached rectangle. All statistics were performed in Excel using the Students T-Test to generate p-values.

Chapter 6

References

Allen, C. and G. G. Borisy (1974). "Structural polarity and directional growth of microtubules of Chlamydomonas flagella." Journal of Molecular Biology **90**(2): 381-402.

Allen, N. and R. Allen (1978). "Cytoplasmic Streaming in Green Plants." Annual Review of Biophysics and Bioengineering **7**: 497-526.

Amos, L. A. (1987). "Kinesin from pig brain studied by electron microscopy." Journal of Cell Science **87**: 105-111.

Amos, L. A. and A. Klug (1974). "Arrangement of Subunits in Flagellar Microtubules." Journal of Cell Science **14**: 523-549.

Bastock, R. and D. St. Johnston (2008). "Drosophila oogenesis." Current Biology **18**(23): R1082-R1087.

Berg, H. (1983). Random Walks in Biology, Princeton University Press.

Berleth, T., M. Burri, G. Thoma, D. Bopp, S. Richstein, G. Frigerio, M. Noll and C. Volhard-Nüsslein (1988). "The role of localization of bicoid RNA in organizing the anterior pattern of the Drosophila embryo." EMBO Journal **7**(6): 1749-1756.

Bourdieu, L., T. Duke, M. B. Elowitz, D. A. Winkelmann, S. Leibler and A. Libchaber (1995). "Spiral defects in motility assays: A measure of motor protein force." Physical Review Letters **75**(1): 176-179.

Brendza, K. M., D. J. Rose, S. P. Gilbert and W. M. Saxton (1999). "Lethal kinesin mutations reveal amino acids important for ATPase activation and structural coupling." Journal of Biological Chemistry **274**: 31506-31514.

Brendza, R. P., L. R. Serbus, J. B. Duffy and W. M. Saxton (2000). "A Function for Kinesin I in the Posterior Transport of oskar mRNA and Staufen Protein." Science **289**: 2120-2122.

Brendza, R. P., L. R. Serbus, W. M. Saxton and J. B. Duffy (2002). "Posterior Localization of Dynein and Dorsal-Ventral Axis Formation Depend on Kinesin in Drosophila Oocytes." Current Biology **12**(17): 1541-1545.

Brewster, D. and R. Jameson (1829). "Some Account of Professor Amici's Discoveries relative to the Motion of Sap in Plants." The Edinburgh Philosophical Journal **2**: 172-177.

Brown, E. H. and R. C. King (1964). "Studies on the events resulting in the formation of an egg chamber in Drosophila melanogaster." Growth **28**: 41-81.

Cai, D., A. D. Hoppe, J. A. Swanson and K. J. Verhey (2007). "Kinesin-1 structural organization and conformational changes revealed by FRET stoichiometry in live cells." Journal of Cell Biology **176**: 51-63.

Cha, B.-J., L. R. Serbus, B. S. Koppetsch and W. E. Theurkauf (2002). "Kinesin I-dependent cortical exclusion restricts pole plasm to the oocyte posterior." Nature Cell Biology **4**: 592-598.

Clark, I., E. Giniger, H. Ruohola-Baker, L. Y. Jan and Y. N. Jan (1994). "Transient posterior localization of a kinesin fusion protein reflects anteroposterior polarity of the Drosophila oocyte." Current Biology **4**(4): 289-300.

Conklin, E. G. (1940). Cell and Protoplasm Concepts: Historical Account. The Cell and Protoplasm. A. R. D. C. V. Taylor, J. M. Luck, C. B. van Niel, and A. Tyler, The American Association for the Advancement of Science: The Science Press.

Cooley, L. and W. E. Theurkauf (1994). "Cytoskeletal Functions During Drosophila Oogenesis." Science **266**: 590-596.

Cooley, L., E. Verheyen and K. Ayers (1992). "chickadee encodes a profilin required for intercellular cytoplasm transport during Drosophila oogenesis." Cell **69**(1): 173-184.

Corti, B. (1774). "Osservazioni microscopiche sulla Tremella e sulla circolazione del fluido in una pianta acquajuola dell' Abate." Lucca **8**.

Coy, D. L., W. O. Hancock, M. Wagenbach and J. Howard (1999). "Kinesin's tail domain is an inhibitory regulator of the motor domain." Nature Cell Biology **1**: E119-E121.

Cummings, M. R. and R. C. King (1969). "The Cytology of the Vitellogenic Stages of Oogenesis in Drosophila melanogaster." Journal of Morphology **128**: 427-442.

Cummings, M. R. and R. C. King (1970). "Ultrastructural changes in nurse cells and follicle cells during late stages of oogenesis in Drosophila melanogaster." Zeitschrift fur Zellforschung und mikroskopische Anatomie **110**(1): 1-8.

Dahlgaard, K., A. A. S. F. Raposo, T. Niccoli and D. St. Johnston (2007). "Capu and Spire Assemble a Cytoplasmic Actin Mesh that Maintains Microtubule Organization in the Drosophila Oocyte." Developmental Cell **13**: 539-553.

Desai, A. and T. Mitchison (1997). "Microtubule polymerization dynamics." Annual Review of Cell and Developmental Biology **13**: 83-117.

Dietrich, K. A., C. V. Sindelar, P. D. Brewer, K. H. Downing, C. R. Cremo and S. E. Rice (2008). "The kinesin-1 motor protein is regulated by a direct interaction of its head and tail." PNAS **105**: 8938-8943.

Emmons, S., H. Phan, J. Calley, W. Chen, B. James and L. Manseau (1995). "cappuccino, a Drosophila maternal effect gene required for polarity of the egg and embryo, is related to the vertebrate limb deformity locus." Genes & Development **9**: 2482-2494.

Ephrussi, A. and R. Lehmann (1992). "Induction of germ cell formation by oskar." Nature **358**(6385): 387-392.

Ewart, A. J. (1896). "On Assimilatory Inhibition in Plants " Journal of the Linnean Society of London, Botany **31**(217): 364-461.

Ewart, A. J. and F. Gotch (1903). On the Physics and Physiology of Protoplasmic Streaming in Oxford, Clarendon Press.

Felgner, H., R. Frank and M. Schliwa (1996). "Flexural rigidity of microtubules measured with the use of optical tweezers." Journal of Cell Science **109**((Pt 2)): 509-516.

Fischer-Vize, J. A. and K. L. Mosley (1994). "Marbles mutants: uncoupling cell determination and nuclear migration in the developing Drosophila eye." Development **120**: 2609-2618.

Gaspar, I., Y. Yu, S. Cotton, D.-H. Kim, A. Ephrussi and M. Welte (2014). "Klar ensures thermal robustness of oskar localization by restraining RNP motility." Journal of Cell Biology **206**(2): 199-215.

Gittes, F., B. Mickey, J. Nettleton and J. Howard (1993). "Flexural rigidity of microtubules and actin filaments measured from thermal fluctuations in shape." Journal of Cell Biology **120**: 923-934.

Gross, S. P. (2003). "Dynactin: coordinating motors with opposite inclinations." Current Biology **13**(8): R320-322.

Gross, S. P., Y. Guo, J. E. Martinez and M. A. Welte (2003). "A Determinant for Directionality of Organelle Transport in Drosophila Embryos." Current Biology **13**: 1660-1668.

Guo, Y., S. Jangi and M. A. Welte (2005). "Organelle-specific Control of Intracellular Transport: Distinctly Targeted Isoforms of the Regulator Klar." Molecular Biology of the Cell **16**: 1406-1416.

Gutzeit, H. (1986). "The role of microtubules in the differentiation of ovarian follicles during vitellogenesis in Drosophila." Roux's Archives of Developmental Biology **195**: 173-181.

Gutzeit, H. O. (1986). "The role of microfiliments in cytoplasmic streaming in Drosophila follicles." Journal of Cell Science **80**: 159-169.

Gutzeit, H. O. and R. A. Koppa (1982). "Time-lapse film analysis of cytoplasmic streaming during late oogenesis of Drosophila." Journal of Embryol. exp. Morph. **67**(101-111).

Hamaguchi, M. S. and Y. Hiramoto (1986). "Analysis of the Role of Astral Rays in Pronuclear Migration in Sand Dollar Eggs by the Colcemid-UV Method." Developmental Growth and Differences **28**(2): 143-156.

Kamitsubo, E. (1966). "Motile protoplasmic fibrils in cells of Characeae." Proceedings of the Japan Academy of Sciences **42**: 640.

Kamitsubo, E. (1972). "Motile protoplasmic fibrils in cells of the Characeae." Protoplasma **74**: 53-70.

Kamiya, N. (1959). Protoplasmic Streaming. Vienna, Austria, Springer-Verlag.

Kamiya, N. (1981). "Physical and chemical basis of cytoplasmic streaming." Annual Review of Plant Physiology **32**: 205-236.

Kamiya, N. and K. Kuroda (1956). "Artificial modification of the osmotic pressure of the plant cell." Protoplasma **46**: 423-436.

Kamiya, N. and K. Kuroda (1975). "Active movement of *Nitella* chloroplasts *in vitro*." Proceedings of the Japan Academy of Sciences **51**: 774-777.

Kim, D.-H., S. L. Cotton, D. Manna and M. Welte (2013). "Novel Isoforms of the Transport Regulator Klar." PLoS One **8**(2): e55070.

Kim-Ha, J., J. L. Smith and P. M. Macdonald (1991). "oskar mRNA is localized to the posterior pole of the Drosophila oocyte." Cell **66**(1): 23-35.

Kimura, K. and A. Kimura (2011). "Intracellular organelles mediate cytoplasmic pulling force for centrosome centration in the Caenorhabditis elegans early embryo." Proceedings of the National Academy of Sciences of the United States of America **108**: 137-142.

King, R. C. (1970). Ovarian development in Drosophila melanogaster, Academic Press.

King, R. C. and R. G. Burnett (1959). "An autoradiographic study of uptake of tritiated glycine, thymidine, and uridine by fruit fly ovaries." Science **129**: 1674-1675.

Koch, E. A. and R. H. Spitzer (1983). "Multiple effects of colchicine on oogenesis in Drosophila: Induced sterility and switch of potential oocyte to nurse-cell developmental pathway." Cell and Tissue Research **228**: 21-32.

Kugler, J.-M. and P. Lasko (2009). "Localization, anchoring and translational control of oskar, gurken, bicoid and nanos mRNA during Drosophila oogenesis." Fly **3**(1): 15-28.

Kühne, W. (1897). "Über die bedeutung des Sauerstoffs für die vitale Bewegung." Zeitschrift für Biologie **36**: 425.

Kural, C., H. Kim, S. Syed, G. Goshima, V. I. Gelfand and P. R. Selvin (2005). "Kinesin and dynein move a peroxisome in vivo: a tug-of-war or coordinated movement?" Science **308**(5727): 1469-1472.

Li, Q., T. Xin, W. Chen, M. Zhu and M. Li (2007). "Lethal(2)giant larvae is required in the follicle cells for formation of the initial AP asymmetry and the oocyte polarity during Drosophila oogenesis." Cell Research **18**: 372-384.

Lin, H., L. Yue and A. C. Spradling (1994). "The Drosophila fusome, a germline-specific organelle, contains membrane skeletal proteins and functions in cyst formation." Development **120**(4): 947-956.

Loewy, A. G. (1949). "A Theory of Protoplasmic Streaming." Proceedings of the American Philosophical Society **93**(4): 326-329.

Longoria, R. A. and G. T. Shubeita (2013). "Cargo transport by cytoplasmic Dynein can center embryonic centrosomes." PLoS One **8**: e67710.

Luby-Phelps, K. (2000). "Cytoarchitecture and physical properties of cytoplasm: volume, viscosity, diffusion, intracellular surface area." International Review of Cytology **192**(189-221).

Magie, C. R., M. R. Meyer, M. S. Gorsuch and S. M. Parkhurst (1999). "Mutations in the Rho1 small GTPase disrupt morphogenesis and segmentation during early Drosophila development." Development **126**(23): 5353-5364.

Mahajan-Miklos, S. and L. Cooley (1994). "Intercellular cytoplasm transport during Drosophila oogenesis." Developmental Biology **165**(2): 336-351.

Manseau, L., J. Calley and H. Phan (1996). "Profilin is required for posterior patterning of the Drosophila oocyte." Development **122**: 2109-2116.

Manseau, L. J. and T. Schüpbach (1989). "cappuccino and spire: two unique maternal-effect loci required for both the anteroposterior and dorsoventral patterns of the Drosophila embryo." Genes & Development **3**(9): 1437-1452.

Máthé, E. (2004). "Immunocytological Analysis of Oogenesis." Methods of Molecular Biology **247**: 89-127.

McDonald, K. (1999). High-Pressure Freezing for Preservation of High Resolution Fine Structure and Antigenicity for Immunolabeling. Methods in Molecular Biology. N. Hajibagheri. Totowa, NJ, Humana Press Inc. . **117**.

Meijering, E. and O. Dzyubachyk (2012). "Methods for Cell and Particle Tracking." Methods of Enzymology **504**: 183-200.

Mosley-Bishop, K. L., Q. Li, K. Patterson and J. A. Fischer (1999). "Molecular analysis of the klarsicht gene and its role in nuclear migration within the differentiating cells of the Drosophila eye." Current Biology **9**: 1211-1220.

Moua, P. K. (2009). Differential functions of the Kinesin-1 tail in Drosophlia transport processes. PhD, University of California Santa Cruz.

Nachmias, V. T. (1969). "Studies on Streaming." Journal of Cell Biology **40**(1): 160-166.

Nagai, R. and L. I. Rebhun (1966). "Cytoplasmic microfilaments in streaming *Nitella* cells." Journal of Ultrastructure Research **14**: 571-589.

Nägeli, C. W. v. (1860). Beiträge zur wissenschaftlichen Botanik.

Neuman-Silberberg, F. S. and T. Schüpbach (1993). "The Drosophila dorsoventral patterning gene gurken produces a dorsally localized RNA and encodes a TGF alpha-like protein." Cell **75**(1): 165-174.

Niwayama, R. and A. Kimura (2012). "A cellular funicular: A hydrodynamic coupling between the anterior- and posterior-directed cytoplasmic flows." Worm **1**: 72-76.

Otto, I. M., T. Raabe, U. E. Rennefahrt, P. Bork, U. R. Rapp and E. Kerkhoff (2000). "The p150-Spir protein provides a link between c-Jun N-terminal kinase function and actin reorganization." Current Biology **10**(6): 345-348.

Palacios, I. M. and D. St. Johnston (2002). "Kinesin light chain-independent function of the Kinesin heavy chain in cytoplasmic streaming and posterior localisation in the Drosophila oocyte." Development **129**: 5473-5485.

Parton, R. M., R. S. Hamilton, G. Ball, L. Yang, C. F. Cullen, W. Lu, H. Ohkura and I. Davis (2011). "A PAR-1-dependent orientation gradient of dynamic microtubules directs posterior cargo transport in the Drosophila oocyte." J Cell Biol **194**(1): 121-135.

Pfeffer, W. (1906). Tropic movements. The physiology of plants: A treatise upon the metabolism and sources of energy in plants. Oxford, Clarendon. **3**.

Pilling, A. D., D. Horiuchi, C. M. Lively and W. M. Saxton (2006). "Kinesin-1 and Dynein are the primary motors for fast transport of mitochondria in Drosophila motor axons." Molecular Biology of the Cell **17**(4): 2057-2068.

Pokrywka, N. J. and E. C. Stephenson (1991). "Microtubules mediate the localization of bicoid RNA during Drosophila oogenesis." Development **113**(1): 55-66.

Purcell, E. M. (1977). "Life at Low Reynolds Number." American Journal of Physics **45**: 3-11.

Riechmann, V. and A. Ephrussi (2001). "Axis formation during Drosophila oogenesis." Current Opinion in Genetic Development **11**(4): 374-383.

Ritter, G. (1899). "Die Abhängigkeit der Protoplasmaströmung und der Geisselbewegung vom freien Sauerstoff." Flora **86**: 329-360.

Robb, J. A. (1969). "Maintenance of imaginal discs of Drosophila melanogaster in chemically defined media." Journal of Cell Biology **41**(3): 876-885.

Serbus, L. R., B.-J. Cha, W. E. Theurkauf and W. M. Saxton (2005). "Dynein and the actin cytoskeleton control kinesin-driven cytoplasmic streaming in Drosophila oocytes." Development **132**(16): 3743-3752.

Sharp, L. W. (1921). An Introduction to Cytology. New York, New York, McGraw-Hall Book Company, Inc.

Shimmen, T. and M. Tazawa (1982). "Cytoplasmic streaming in the cell model *Nitella*." Protoplasma **112**: 101-106.

Shinar, T., M. Manab, F. Piano and M. J. Shelley (2011). "A model of cytoplasmically driven microtubule-based motion in the single-celled Caenorhabditis elegans embryo." PNAS **108**(26): 10508-10513.

Shubeita, G. T., S. L. Tran, J. Xu, M. Vershinin, S. Cermelli, S. L. Cotton, M. A. Welte and S. P. Gross (2008). "Consequences of Motor Copy Number on the Intracellular Transport of Kinesin-1-Driven Lipid Droplets." Cell **135**: 1098-1107.

St. Johnston, D., D. Beuchle and C. Nüsslein-Volhard (1991). "Staufen, a gene required to localize maternal RNAs in the Drosophila egg." Cell **66**(1): 51-63.

Starr, D. A. and M. Han (2002). "Role of ANC-1 in tethering nuclei to the actin cytoskeleton." Science **298**(5592): 406-409.

Storto, P. D. and R. C. King (1989). "The role of polyfusomes in generating branched chains of cystocytes during Drosophila oogenesis." Developmental Genetics **10**(2): 70-86.

Svoboda, K. and S. M. Block (1994). "Force and velocity measured for single kinesin molecules." Cell **77**(5): 773-784.

Theurkauf, W. E. (1994). "Microtubules and Cytoplasm Organization during Drosophila Oogenesis." Developmental Biology **165**: 352-360.

Theurkauf, W. E. (1994). "Premature Microtubule-Dependent Cytoplasmic Streaming in cappuccino and spire
Mutant Oocytes." Science **265**: 2093-2096.

Theurkauf, W. E., B. M. Alberts, Y. N. Jan and T. A. Jongens (1993). "A central role for microtubules in the differentiation of Drosophila oocytes." Development **118**: 1169-1180.

Theurkauf, W. E. and R. S. Hawley (1992). "Meiotic spindle assembly in Drosophila females: behavior of nonexchange chromosomes and the effects of mutations in the nod kinesin-like protein." Journal of Cell Biology **116**(5): 1167-1180.

Theurkauf, W. E., S. Smiley, M. L. Wong and B. M. Alberts (1992). "Reorganization of the cytoskeleton during Drosophila oogenesis: implications for axis specification and intercellular transport." Development **115**(923-936).

Thurston, W. (1988). "On the geometry and dynamics of diffeomorphisms of surfaces." Bulletin of the American Mathematical Society **19**: 417-431.

Vale, R. D. and R. J. Fletterick (1997). "The design plan of kinesin motors." Annual Review of Cell and Developmental Biology **13**: 745-777.

Vale, R. D. and R. A. Milligan (2000). "The way things move: looking under the hood of molecular motor proteins." Science **288**(5463): 88-95.

Vale, R. D., T. S. Reese and M. P. Sheetz (1985). "Identification of a novel force-generating protein, kinesin, involved in microtubule-based motility." Cell **42**(1): 39-50.

Verheyen, E. M. and L. Cooley (1994). "Profilin mutations disrupt multiple actin-dependent processes during Drosophila development." Development **120**(4): 717-728.

Wang, S. and T. Hazelrigg (1994). "Implications for bcd mRNA localization from spatial distribution of exu protein in Drosophila oogenesis." Nature **369**(6479): 400-403.

Wang, Y. and V. Riechmann (2008). "Microtubule anchoring by cortical actin bundles prevents streaming of the oocyte cytoplasm." Mechanisms of Development **125**: 142-152.

Warn, R. M., H. O. Gutzeit, L. Smith and A. Warn (1985). "F-Actin Rings are Associated with the Ring Canals of the Drosophila Egg Chamber." Experimental Cell Research **157**: 355-363.

Wellington, A., S. Emmons, B. James, J. Calley, M. Grover, P. Tolias and L. Manseau (1999). "Spire contains actin binding domains and is related to ascidian posterior end mark-5." Development **126**(5267-5274).

Welte, M. A. (2004). "Bidirectional Transport along Microtubules." Current Biology **14**: R525-R537.

Welte, M. A., S. P. Gross, M. Postner, S. M. Block and E. F. Wieschaus (1998). "Developmental Regulation of Vesicle Transport in Drosophila Embryos: Forces and Kinetics." Cell **92**: 547-557.

Wheatley, S., S. Kulkarni and R. Karess (1995). "Drosophila nonmuscle myosin II is required for rapid cytoplasmic transport during oogenesis and for axial nuclear migration in early embryos." Development **121**: 1937-1946.

Wieschaus, E. and C. Nüsslein-Volhard (1986). Looking at Embryos. Drosophila: A Practical Approach. D. B. Roberts. Oxford, IRL Press**:** 199-227.

Wolke, U., E. A. Jezuit and J. R. Priess (2007). "Actin-dependent cytoplasmic streaming in C. elegans oogenesis." Development **134**: 2227-2236.

Yi, K., B. Rubinstein, J. R. Unruh, F. Guo, B. D. Slaughter and R. Li (2013). "Sequential actin-based pushing forces drive meiosis I chromosome migration and symmetry breaking in oocytes." Journal of Cell Biology **200**(5): 567-576.

Yi, K., J. R. Unruh, M. Deng, B. D. Slaughter, B. Rubinstein and R. Li (2011). "Dynamic maintenance of asymmetric meiotic spindle position through Arp2/3-complex-driven cytoplasmic streaming in mouse oocytes." Nature Cell Biology **13**(10): 1252-1260.

Yu, Y. V., Z. Li, N. P. Rizzo, J. Einstein and M. A. Welte (2011). "Targeting the motor regulator Klar to lipid droplets." BMC Cell Biology **12**(9): 15 pages.

Zimyanin, V. L., K. Belaya, J. Pecreaux, M. J. Gilchrist, A. Clark, I. Davis and D. St. Johnston (2008). "In Vivo Imaging of oskar mRNA Transport Reveals the Mechanism of Posterior Localization." Cell **134**: 843-853.